

UNCLASSIFIED
CLASSIFICATION OF THIS PAGE

REPORT DOC

AD-A263 048

1. REPORT SECURITY CLASSIFICATION

DTIC
ELECTE

2. SECURITY CLASSIFICATION AUTHORITY

3. DECLASSIFICATION/DOWNGRADING SCHEDULE

APR 1 1993

4. PERFORMING ORGANIZATION REPORT NUMBER(S)

C

S D

Approved for public release;
distribution unlimited.

5. MONITORING ORGANIZATION REPORT NUMBER(S)

AFOSR TR 11100

7a. NAME OF MONITORING ORGANIZATION

Air Force Office of Scientific Research/NE

6a. NAME OF PERFORMING ORGANIZATION

Northwestern University

6b. OFFICE SYMBOL
(If applicable)

NE

7b. ADDRESS (City, State, and ZIP Code)

Dept. of Materials Science and Engineering
Evanston, IL 60208-3108

Building 410

Bolling AFB, DC 20332-6448

8a. NAME OF FUNDING SPONSORING
ORGANIZATION

AFOSR

8b. OFFICE SYMBOL
(If applicable)

9. PROCUREMENT INSTRUMENT IDENTIFICATION NUMBER

AFOSR-89-0043

10. ADDRESS (City, State, and ZIP Code)

Building 410
Bolling AFB, DC 20332-6448

10. SOURCE OF FUNDING NUMBERS

PROGRAM ELEMENT NO	PROJECT NO	TASK NO	WORK UNIT ACCESSION NO
61102F	2306	A1	-

11. TITLE (Include Security Classification)

Tailored Interfaces for Metal-Matrix Composites-Fundamental Considerations

12. PERSONAL AUTHOR(S)

Morris E. Fine and Julia R. Weertman

13a. TYPE OF REPORT
Final Technical

13b. TIME COVERED
FROM 10/1/88 TO 11/30/91

14. DATE OF REPORT (Year, Month, Day)
January 28, 1993

15. PAGE COUNT

16. SUPPLEMENTARY NOTATION

17. COSATI CODES

FIELD	GROUP	SUB-GROUP

18. SUBJECT TERMS (Continue on reverse if necessary and identify by block number)

Metal matrix composites, interfaces, aluminum matrix, magnesium matrix, titanium carbide, silicon carbide, spinel

19. ABSTRACT (Continue on reverse if necessary and identify by block number)

The objective of this research was to investigate the interface properties needed for successful metal matrix composites. Thermodynamic stability of the interface and the phases in the composite, nature of the bonding across the interface, and the energy and structure of the interface were studied. With TiC dispersed in Al prepared by the XD process, atomic resolution electron microscopy showed a sharp interface with large areas of partial coherence. The Al-TiC composite is remarkably ductile even at 15 vol.% TiC loading. This attributed to the ability of the Al to recrystallize at the interface forming semicoherent boundaries and to a high level of metallic binding between Al and Ti in TiC. On holding at 640 C the kinetics of the reaction, 13Al + 3TiC \rightarrow Al₄C₃ + 3Al₃Ti, is rapid enough to be observed. This reaction leads to a substantial increase in strength and modulus but a reduction in ductility. Like steel, parts could be formed in the ductile state and then heat treated to increase hardness and modulus. At still higher temperatures, Al and TiC are the thermodynamically stable phases so no reaction occurs. Four Mg alloy matrix composites were received from Dow Chemical Corp.:

20. DISTRIBUTION/AVAILABILITY OF ABSTRACT

UNCLASSIFIED/UNLIMITED SAME AS RPT DTIC USERS

21. ABSTRACT SECURITY CLASSIFICATION

22a. NAME OF RESPONSIBLE INDIVIDUAL

Dr. Alan H. Rosenstein

22b. TELEPHONE (Include Area Code)

(202) 767-4960

22c. OFFICE SYMBOL

NE

DO FORM 1473, 84 MAR

83 APR edition may be used until exhausted.
All other editions are obsolete.

SECURITY CLASSIFICATION OF THIS PAGE

UNCLASSIFIED

Reproduced From
Best Available Copy

19. (continued)

Mg-6% Zn with SiC, Mg-3% Ce-1% Mn with SiC, Mg-9% Al-1% Zn with SiC, and Mg-9% Al-1% Zn with Al_2O_3 . All particle matrix interfaces appeared to be incoherent. Reaction of the dispersoids with the matrix were investigated by holding at 500 C for various lengths of time. At this temperature, Mg reacted with SiC to form Mg_2Si plus carbon. The presence of Ce leads to formation of Ce_2C_3 in the interface region. The presence of Al in the alloy gives Al_4C_3 in the reaction zone. Even though Mg is expected to react with Al_2O_3 to form MgO , none was found on long time exposure at 500 C. All reactions degrade modulus, strength, and ductility. With Al-3% Mg matrix composites with alumina ($\alpha\text{-Al}_2\text{O}_3$) and spinel (MgAl_2O_4) dispersoids prepared by mechanical alloying and extrusion, the spinel particles end up being much smaller and better dispersed than the alumina particles even though the starting size is larger. The creep resistance increases substantially with volume fraction dispersoid in both composite systems following threshold type behavior. The threshold stress decreases substantially on heating; for example, 280 to 110 MPa on heating the 25 vol.% spinel composite from 225 to 425 C. The reaction of Mg with $\alpha\text{-Al}_2\text{O}_3$ occurs during processing. The natural occurring composite of Al matrix with 15 to 25 vol.% tetragonal $\text{Al}_3\text{Zr}_{1-x}\text{Ti}_x$ intermetallic dispersoids prepared by solidification from the melt was cold rolled to greater than 95% reduction. This remarkable ductility is thought to have the same origin as in Al-TiC, that is, recrystallization of the Al matrix at the interfaces and a high degree of metallic binding. One of the major conclusions of this research was that MMCs with good ductility can be made in a number of systems if interfacial contamination is avoided so that the matrix can form an unobstructed interface with the dispersed phase.

DTIC QUALITY INDEXED 4

Accession For	
NTIS CRA&I	<input checked="" type="checkbox"/>
DTIC TAB	<input type="checkbox"/>
Unannounced	<input type="checkbox"/>
Justification	
By _____	
Distribution / _____	
Availability Codes	
Dist	Avail and/or Special
A-1	

93-06636



Q9P8

99 3 31 075

DEPARTMENT OF MATERIALS SCIENCE AND ENGINEERING
McCORMICK SCHOOL OF ENGINEERING AND APPLIED SCIENCE
NORTHWESTERN UNIVERSITY
EVANSTON, IL 60208

Final Technical Report on

Tailored Interfaces for Metal-Matrix Composites-
Fundamental Considerations

to

Electronic and Solid State Sciences Division
Air Force Office of Scientific Research
Bolling Air Force Base
Washington, DC 20332
Attn: Dr. Alan H. Rosenstein
AF Grant No.: AFOSR-89-0043

For the Period
1 October 1988 to 30 November 1992

Principal Investigators

Morris E. Fine, Walter P. Murphy Professor of Materials
Science and Engineering
Julia R. Weertman, Walter P. Murphy Professor of Materials
Science and Engineering

15 December 1992

Approved for public release;
distribution unlimited.

TABLE OF CONTENTS

	<u>Pg. No.</u>
PROFESSIONAL PERSONNEL	i
STATEMENT OF WORK	ii
SUMMARY	iii
PUBLICATIONS FROM THIS RESEARCH	vi
INTRODUCTION	1
I. Mechanical and Interfacial Properties of α -Alumina and Spinel Dispersed Al-based Composites	4
II. Magnesium Metal Matrix Composites	29
III. Microstructure and Interfaces in XD Al-TiC Metal Matrix Composites	57
IV. Ductility of Cast Al-Al ₃ Zr _x Ti _{1-x} Composites	87

PROFESSIONAL PERSONNEL

Professor Morris E. Fine, Principal Investigator

Professor Julia R. Weertman, Principal Investigator

John Blum, PhD Student, Graduate Research Assistant,
finished experimental research, left for U. S.
Can Company 7/1/91, final exam scheduled for
later in 1993.

Neil R. Brown, PhD Student, Graduate Research Assistant,
finished November 1992, accepted Postdoctoral
position, Chemical Technology Division, Argonne
National Laboratory, Argonne, IL.

Philip A. Earvolino, Fellowship student, completed MS
degree January 1992, employed at Spire Corporation,
Bedford, MA 01730 in technical sales.

Rahul Mitra, PhD Student, Graduate Research Assistant,
finished November 1992, accepted Scientist "C"
position at Defence Metallurgical Research Lab.,
Hyderabad 500258, India.

STATEMENT OF WORK

Synthetic MMCs have a number of attractive features. It appears possible to design a composite material which meets specified criteria by a suitable choice of phases. However, whether or not the material actually is satisfactory depends in large part on the nature of the interface between the matrix and the other phase or phases and the chemical reactions which may occur. In this research a number of properties of the interfaces in selected MMCs which have a strong bearing on performance were investigated. These properties include the thermodynamic stability of the interface region and the phases in the composite, the nature of the interfacial bonding, and the degree of coherence at the interface. It was the goal of this research to obtain basic information about those aspects of the interface to assist in formulation of general principles to guide the tailoring of interfaces in MMCs in order to obtain optimum performance. Because of the complexity of interfaces, atomic resolution techniques were needed to study them in detail. Interfaces in a number of selected MMCs were investigated down to an atomic scale to answer questions about the interface structure and chemistry.

SUMMARY

The objective of this research was to investigate the interface properties needed for successful metal matrix composites. A number of factors were selected for study. These are thermodynamic stability of the interface and the phases in the composite, nature of the bonding across the interface, and the energy and structure of the interface.

TiC was chosen as a dispersant for an Al matrix MMC and composite prepared by the XD process was received from Martin-Marietta in the as-extruded condition. Atomic resolution electron microscopy showed a sharp interface with large areas of partial coherence. Cold working and recrystallization at 500°C resulted in many Al subgrains which were partially coherent with areas of TiC particles. The Al-TiC composite is remarkably ductile even at 15 vol.% TiC loading. This was attributed to the ability of the Al to recrystallize at the interface forming semicoherent boundaries and to a high level of metallic binding between Al and Ti in TiC. While there was no evidence of chemical reaction on holding at 500°C, at 640°C the kinetics of the reaction, $13\text{Al} + 3\text{TiC} \rightarrow \text{Al}_4\text{C}_3 + 3\text{Al}_3\text{Ti}$, is rapid enough to be observed after many hours. There is partial coherence between phases in the reaction zone. The reaction leads to a substantial increase in strength and modulus but a reduction in ductility. Like steel, parts could be formed in the ductile state and then heat treated to increase hardness and modulus. At still higher temperatures, Al and TiC are the thermodynamically stable phases so that the composite is readily prepared in molten Al.

Four Mg alloy matrix composites were received from Dow Chemical Corporation: Mg-6% Zn with SiC, Mg-3% Ce- 1% Mn with SiC, Mg-9% Al-1% Zn with SiC, and Mg-9% Al-1% Zn with Al_2O_3 . These were prepared by stirring the dispersoid

into molten alloy and casting. The first two alloys were extruded after casting. These two composites elongated about 5% in tensile tests while the as-cast Mg-9% Al-1% Zn composites were considerably more brittle. All particle matrix interfaces appeared to be incoherent. Reaction of the dispersoids with the matrix were investigated by holding at 500°C for various lengths of time. At this temperature, Mg reacted with SiC to form Mg₂Si plus carbon. The presence of Ce leads to formation of Ce₂C₃ in the interface region. The presence of Al in the alloy gives Al₄C₃ in the reaction zone. Even though Mg is expected to react with Al₂O₃ to form MgO, none was found on long time exposure at 500°C. All reactions led to degradation of modulus, strength, and ductility.

With Al-3% Mg matrix composites with alumina (α -Al₂O₃) and spinel (MgAl₂O₄) dispersoids prepared by mechanical alloying and extrusion, the spinel particles end up being much smaller than the alumina particles even though the starting size is larger. At 10 vol.% loading the smaller particle size doubles the creep resistance but at 25 vol.% loading both composites have approximately the same creep resistance. The creep resistance increases substantially with volume fraction dispersoid in both composite systems. At 225 to 425°C, the flow stress vs. strain rate for both systems follows a threshold type behavior, below a certain strain rate the flow stress is independent of strain rate. The threshold stress decreases substantially on heating; for example, 280 to 110 MPa on heating the 25 vol.% spinel composite from 225 to 425°C.

With Al-3% Mg/ α -Al₂O₃ composites, the reaction of Mg with α -Al₂O₃ occurs in processing. There is evidence of partial coherence in the reaction zone as seen by atomic resolution TEM. The 3% Mg in the matrix alloy appears to improve the bonding of the matrix with the α -Al₂O₃.

The natural occurring composite of Al matrix with 15 to 25 vol.% tetragonal $Al_3Zr_{1-x}Ti_x$ intermetallic dispersoids prepared by solidification from the melt can be cold rolled to 95% reduction or more. This remarkable ductility is thought to have the same origin as in Al-TiC, that is, recrystallization of the Al matrix at the interfaces and a high degree of metallic binding.

One of the major conclusions of this research was that MMCs with good ductility can be made in a number of systems if interfacial contamination is avoided so that the matrix can form an unobstructed interface with the dispersed phase.

PUBLICATIONS FROM THIS RESEARCH

I. Published

Relaxation Mechanisms at the Interfaces in the XD™ Al/TiC_p Metal Matrix Composites, by R. Mitra, W. A. Chiou, J. R. Weertman and M. E. Fine, *Scripta Met. et Mat.* 25, pp. 2689-2694 (1991).

Study of Interfaces in XD™ Al/TiC_p Metal Matrix Composites, by R. Mitra, W. A. Chiou, J. R. Weertman, M. E. Fine and R. M. Aikin, Jr., *Mat. Res. Soc. Symp.* Vol. 238 (1992) Materials Research Society, Pittsburgh, PA, pp. 871-876.

Processing an Al/Al₃Zr_{0.25}Ti_{0.75} Metal-Matrix Composite by Conventional Melting, Casting and Rolling, by P. A. Earvolino, M. E. Fine, J. R. Weertman and V. R. Parameswaran, *Scripta Met. et Mat.* 26, pp. 945-948 (1992).

Modification of Microstructure and Mechanical Properties of XD™ Al/TiC Composites by 913 K Exposure, by R. Mitra, J. R. Weertman, M. E. Fine and R. M. Aikin, Jr., chapter in *Proc. of TMS Symposium Developments in Ceramic and Metal-Matrix Composites* (K. Upadhyay, ed.) The Minerals, Metals and Materials Society (TMS), Warrendale, PA (1991) pp. 125-142.

II. Submitted

Chemical Reaction Strengthening of Al/TiC Metal Matrix Composites by Isothermal Heat Treatment at 913 K, by R. Mitra, M. E. Fine and J. R. Weertman. Submitted to the *Journal of Materials Research*.

Interfaces in Metal Matrix Composites Prepared by In-Situ Processing, by R. Mitra, M. E. Fine and J. R. Weertman. Submitted to *Zeitschrift fur Metallkunde*.

Effects of Thermal Exposure and Interfacial Reaction Zones on the Mechanical Properties of Magnesium-Alloy Metal Matrix Composites, by N. B. Brown, M. E. Fine and J. R. Weertman. Submitted to the *Journal of Materials Research*.

Interfaces in As-Extruded XD Al/TiC and Al/TiB₂ Metal Matrix Composites, by R. Mitra, W. A. Chiou, M. E. Fine and J. R. Weertman. Submitted to the *Journal of Materials Research*.

Effect of Deformation on the Matrix and Interface Microstructure of XD Al/TiC Metal Matrix Composites, by R. Mitra, M. E. Fine and J. R. Weertman. Submitted to the *Journal of Materials Research*.

III. In Preparation

Mechanical and Interfacial Properties of α -Alumina and Spinel Dispersed Al-Based Composites, by J. J. Blum, J. R. Weertman and M. E. Fine.

INTRODUCTION

While synthetic MMCs have a number of attractive features, whether or not the material actually is satisfactory depends in large part on the nature of the interface between the matrix and the other phase or phases. The purpose of this research was to study, in as general a fashion as possible, properties of the interfaces in MMCs such as thermodynamic stability, the degree of coherency between the matrix and other phase lattices, the nature of the reaction zone, and solute segregation. The goal was to obtain basic information about the interface to guide tailoring of interfaces in MMCs to obtain optimum performance. Because of the complexity of interfaces, as well as the need for atomic resolution techniques to study them in detail, many questions remain about their structure, chemistry, and behavior under service conditions. This study of interfaces aims to relate the structure and chemistry to the behavior of material in the boundary region as well as to the composite as a whole.

The main body of this report consists of four individual reports.

- I. Mechanical and Interfacial Properties of Spinel and α -Alumina Dispersed Aluminum-Based Composites, John J. Blum
- II. Magnesium Metal Matrix Composites, Neil R. Brown
- III. Study of Interface in Al/TiC Metal Matrix Composites, Rahul Mitra
- IV. Ductility of Cast Al-Al₃Zr_xTi_{1-x} Composites, Phil Earvolino

The results of this research of importance to development of improved metal matrix composites are now summarized.

1. In-situ processing, such as formation of the reinforcing phase by exothermic reaction in a liquid phase (e.g., TiC in aluminum) can lead to clean interfaces with direct contact on an atomic level between matrix and reinforcing phase. Low energy interfaces can form which maximize the atoms interacting to form chemical bonds. These interfaces can form during solidification or during deformation. Dynamic recovery during forming, such as cold rolling of Al-TiC composite, can result in matrix sub-grains which are in semicoherent relationship with the matrix. A high degree of metallic bonding across interfaces is desirable to obtain fracture-tough interfaces. The combination of metallic bonding and the accommodation of deformation by recovery of the matrix at the interface allows Al-TiC composite with 15 vol.% TiC to be cold rolled to more than 90% reduction without annealing.
2. While the above conclusions were mainly reached by investigation of Al-TiC and 2024 Al alloy-TiB₂ MMCs, these conclusions are reinforced by results for an Al matrix - 15 vol.% Al₃Zr_{0.25}Ti_{0.75} composite formed by casting. It was cold rolled with intermediate anneals to a total reduction in thickness of over 99%.
3. Chemical reaction between phases such as between Al and TiC below 1025 K, where Al₃Ti and Al₄C₃ are formed as products, can lead to substantial increases in elastic modulus and low and high temperature strengths with sacrifice of ductility. Fabrication in the ductile state followed by heat treatment to increase strength, such as done with steel, should be of interest.
4. Composites of Al-3% Mg strengthened with 10 and 25 vol.% α -Al₂O₃ or spinel (MgAl₂O₄) were prepared by ball milling and hot extrusion, and their room and high temperature properties were investigated and compared. During

ball milling, the spinel particle size is reduced much more than that of the α -alumina, giving a finer and more uniform dispersion in the spinel composite. As a result, for the same volume fraction of dispersoid, the room temperature strength of the spinel composite is substantially improved over that of the Al_2O_3 material. This creep strength advantage persists to higher temperatures for 10 vol.% of dispersoid but disappears at 425 °C for 25 vol.% dispersoid. In the Al-3% Mg- $\alpha\text{Al}_2\text{O}_3$ composite, a reaction zone consisting of Mg₂Si or spinel forms at the interface. Both composites, with 10 or 25 vol.% of dispersoid, have low fracture toughness. This behavior is attributed to the polar nature of the atom bonds across the interface, together with the large number of particles sited at grain boundaries. All interfaces are incoherent.

5. In magnesium alloy matrix composites prepared by introducing SiC or $\alpha\text{-Al}_2\text{O}_3$ powder into the melt, there was no indication of a chemical reaction zone using conventional transmission electron microscopy. However, holding at 773 K for a long time resulted in reduction of SiC to form Mg_2Si and a reaction zone was observed. Addition of Ce led to the formation of CeC, as well. These reactions degraded strength, modulus and ductility. The loss in performance was attributed to cracking at the interphase interfaces, probably due to coefficient of expansion mismatches among the phases.

I. MECHANICAL AND INTERFACIAL PROPERTIES OF α -ALUMINA AND SPINEL DISPERSED Al-BASED COMPOSITES, J. J. Blum

Introduction

Dispersion strengthening of aluminum by α -alumina has been extensively studied previously and has been shown to significantly increase strength (1). However, spinel ($MgAl_2O_4$) as a dispersoid has not been as thoroughly studied. Creasy et al. (2) have shown spinel to be a more effective dispersoid than alumina in an aluminum-matrix composite at low oxide volume fractions. The present investigation studied and compared the mechanical and interfacial properties of an aluminum + 3% magnesium matrix mechanically alloyed with nominal 10 and 25 oxide volume percent of either α -alumina or spinel as a function of strain rate and temperature up to 425 C (3/4 T_m). The 3% Mg-Al matrix was chosen so that the oxide formed during processing might be spinel and also to give better bonding between the matrix and α - Al_2O_3 by forming a reaction layer. Temperature dependent strengthening mechanisms are analyzed and discussed. An interfacial reaction zone around alumina particles was also noted and investigated.

Experiment

Elemental powders of Al + 3% Mg and 10 and 25 vol.% α -alumina or spinel were combined in a Spex Model 8000 Ball Mill and mechanically alloyed. To avoid contamination, no surfactant was used. The initial and final dispersoid particle sizes are given in Table I. After milling, the powders were vacuum degassed at 350 C and 10^{-5} torr and pressed to remove porosity and then hot extruded at 400 C at an extrusion ratio of 20:1 into 10 mm diameter rods. Cylindrical shaped specimens were machined from the extruded rods and

tested for elastic modulus using a non-destructive acoustic wave resonance technique (3). Coefficients of thermal expansion were also determined on cylindrical specimens in the temperature range 93 to 204 C. Additionally, cylindrical compression specimens 9 mm in height and 6 mm in diameter were machined from the extruded rods. Compression tests were performed under strain rate control on an Instron Model 1150 Servo-Hydraulic Testing Machine equipped with a vacuum furnace and an axial extensometer. Strain rates were varied between 10^{-1} s⁻¹ to 10^{-6} s⁻¹ at room temperature, 225, 325 and 425 C.

Oxide volume fraction, oxide particle size and matrix grain size and structure were analyzed using thinned foils and extraction replicas on a Hitachi H-700H conventional TEM operating at 200 kV. TEM foils were prepared by mechanical thinning to thicknesses of approximately 10-20 μ m and final polishing and perforation was done by ion milling in a liquid nitrogen cooled state. Analytical and high resolution microscopy studies were performed on a Hitachi HF-200 and a Hitachi H-9000, respectively.

Results and Discussion

To characterize the microstructural differences among the Al-10 vol.% alumina, Al-10 vol.% spinel, Al-25 vol.% spinel and Al-25 vol.% alumina composites, a comprehensive microscopic investigation was performed. First, the actual rather than the nominal oxide volume fractions were determined from extraction replicas by lineal analysis. Although the nominal oxide volume fractions were identical at 10 and 25 volume percent, the aluminum powder oxidizes during mechanical alloying and this depends on the time of mechanical alloying. Therefore, the actual oxide volume fractions are larger. As shown in Table 1 these were 12 and 15 volume

percent for Al-10 vol.% alumina and Al-10 vol.% spinel and 28 and 30 volume percent for Al-25 vol.% alumina and Al-25 vol.% spinel, respectively. The higher oxide content in the Al-10 vol.% spinel composite may be attributed to the longer mechanical alloying period than for the Al-10 vol.% alumina composite. The 25 volume percent composites were mechanically alloyed for identical periods but still the spinel composite gave the larger volume fraction.

The initial particle sizes as well as the final particle sizes after mechanical alloying are shown in Table 1. These were also determined from extraction replicas. Although the initial spinel particle size in the 10 volume percent composite was larger than the average α -alumina particle size, the final size is smaller. The spinel particles were reduced during mechanical alloying while the α -alumina particle size remained relatively constant so that the alumina particles are 8 times larger than the spinel particles. Spinel has a (111) cleavage plane habit which facilitates the fracturing of spinel particles during the mechanical alloying process. The smaller spinel particles compared to the alumina particles results in a smaller interparticle spacing and a smaller grain size, which should result in a higher flow stress. When fabricating the 25 volume percent composites, alumina with a very small grain size was utilized so that final particle sizes of the two composites after mechanical alloying would be more similar; however, the alumina particles are still 4 times larger than the spinel particles.

Since the grain diameter of dispersion strengthened materials is often submicron, dark field TEM micrographs were used to determine the average grain size of the composites. Due to the hot extrusion consolidation process, the grains were elongated parallel to the extrusion

direction yet equiaxed transverse to the extrusion direction. Grain size measurements were made both perpendicular and parallel to the extrusion direction. Average grain size was determined by measuring perpendicular diameters and taking the square root of their product:

$$D_{av} = (D_1 D_2)^{\frac{1}{2}}. \quad (1)$$

Average grain sizes for all four composites are shown in Table 2.

The elastic Young's moduli of the four composites were determined and compared to simple rules of mixtures in Fig. 1. The Voight modulus assumes constant strain (isostrain) throughout the composite and is given by:

$$M_v = xM_A + yM_B \quad (2)$$

and the Reuss modulus assumes constant stress (isostress) throughout the composite and is given by

$$M_r = (x/M_A + y/M_B)^{-1} \quad (3)$$

where x and y are volume fraction of phase A and phase B and M_A and M_B are the Young's moduli of phase A and phase B. Data for the non-dispersed matrix was also determined by performing similar acoustic wave resonance tests on a Al + 3% Mg cold rolled sample, and numerical values for 100% oxides was obtained from Hertzberg (4). Figure 1 graphically depicts the ratio of measured modulus to predicted modulus. The measured Young's moduli are close to those predicted by the Reuss-isostress averaging. Previously, one of the authors (Fine) came to the same conclusion based on literature data for Young's modulus of Al_2O_3 -Al metal matrix composites (4). Due to the high moduli of the α -alumina and spinel compared to Al, the strains in the oxides will be less than those in the matrix and the isostress assumption is a better approximation.

Dilatometry of the composites was performed in the temperature range of 93 to 240 C. Coefficients of thermal expansion were determined by making a least-squares approximation of the slope of the measured length change versus temperature plot. The results of dilatometry testing on the four composites are detailed in Table 4 and Fig. 2. The plot of measured and predicted CTEs shows the spinel composites to behave according to the linear law of mixtures while the alumina composites are slightly below.

The interface between the oxides and the matrix was investigated by transmission electron microscopy. Electron diffraction showed no orientation relationship between either spinel or α -alumina and the matrix. Further investigation of the interface at high magnification revealed a reaction zone around the alumina particles. Conversely, the spinel particles showed no evidence of a new phase in the interface with the aluminum + 3% magnesium matrix. Figure 3 shows the reaction zone as seen in an extraction replica micrograph. The reaction zone is clearly visible around the alumina particles. Figure 4 shows the reaction zone around alumina particles in the Al + 3% Mg matrix as seen by transmission electron microscopy. The magnesium in the Al + 3% Mg alloy reduces α -alumina according to the following equation:



which occurs both during sintering at 350 C and at the hot extrusion temperature (400 C) where the Gibbs free energy for the reaction, $\Delta G = -121$ kJ/mole. The magnesium oxide further reacts with the remaining alumina to form spinel according to Eq.(2):



which again may form at 350 and 400 C ($\Delta G = -24.9$ kJ/mole).

The reaction zone was further investigated by high resolution microscopy. With this technique, the interface was analyzed at the atomic level. Figure 5 shows the reaction zone at the particle/matrix interface. The interface consists of numerous crystallites approximately 60 nm in diameter. Figure 6 shows a higher magnification micrograph of the reaction zone detailing the varying orientation of the crystallites.

The reaction zone was also investigated using an analytical microscope. X-ray spectra were taken from five points across the particle/matrix interface. The results of the x-ray point analyses are shown in Fig. 7(a-e). Figure 7a is the spectra from the center of the alumina particle away from the reaction zone. Figure 7b was taken at the particle/reaction zone interface, Figure 7c from the middle of the reaction zone, Figure 7d from the matrix/reaction zone interface and Figure 7e from the matrix. Note that the magnesium, as determined by the area under the peak, increases as the probe approaches the matrix/reaction zone interface and then decreases in the matrix. Figure 8 is a schematic diagram of the reaction zone and the magnesium and aluminum concentration across the reaction zone. The presence of a large magnesium concentration at the reaction zone/matrix interface and then decreasing amounts through the reaction zone substantiates the magnesium reduction of alumina to form MgO and/or spinel. The reaction zone is probably responsible for the coefficient of expansion being less than that predicted by the linear law of mixtures. It assures strong chemical bonding across the interface.

The fabricated composites were creep tested in compression at room temperature, 225, 325 and 425 C at varying strain rates from 10^{-1} to 10^{-6} s^{-1} . Figure 9 shows the results of compression testing at room temperature and 225 C ($0.53T_m$) for both 10 volume percent alumina and 10

volume percent spinel composites. Room temperature strengths are basically independent of strain rate over the range tested. However, the compressive flow stress of the 10 volume percent spinel composite is 530 MPa versus 360 MPa for 10 volume percent alumina. The nearly 50% strength difference between 10 volume percent spinel is maintained at 225 C; however, at 225 C, the compressive flow stress is strain rate dependent from 10^{-1} to 10^{-6} s^{-1} .

Figure 10 shows the results of compression creep testing at 325 C ($0.64T_m$) and 425 C ($0.75T_m$). The nearly 50% strength advantage of Al-spinel over Al-alumina is also maintained at these high temperatures. The compressive flow stresses at 325 C and 425 C are strain rate dependent but the dependence decreases toward a threshold as the strain rate is reduced. Threshold stress behavior has been often noted in the past in dispersion strengthened aluminum alloy systems (6-8).

Figure 11 shows the results of compression testing on 25 volume percent spinel and 25 volume percent alumina composites at room temperature and 225 C. The room temperature compressive flow stresses, 697 and 634 MPa for 25 volume percent spinel and 25 volume percent alumina, respectively, are independent of strain rate over the range tested and only about 10% different. Again, the flow stresses are strain rate dependent at 225 C. Figure 12 presents the results of compression creep testing on the 25 oxide volume percent composites at 325 and 425 C. As with the 10 volume percent oxide composites, the high temperature flow stresses reveal threshold type stress behavior.

Strain rate independence of the flow stress is expected at room temperature where the expected controlling deformation mechanism is the bypass of obstacles such as by Orowan looping (9). At intermediate temperatures, $T = 225$ C ($0.53T_m$), the deformation mechanism appears to

change to a climb and glide of dislocation over hard, non-shearable particles (10). However, at high temperatures, $T > 0.6T_m$, the ability for the deviatoric stress to relax around a hard particle with an incoherent interface is increased sufficiently so that the particle attracts the dislocation to the particle/matrix interface. At the particle/matrix interface, the dislocation can attain a lower energy state by "spreading" out its core (11). The threshold stress is then the stress required to detach the dislocations from the particles.

In creep controlled by threshold type behavior, the strain rate $\dot{\epsilon}$ is expected to follow the equation

$$\dot{\epsilon} = A(\sigma - \sigma_t)^m \exp(-Q/RT) . \quad (6)$$

By taking ratios, an equation with only two unknowns can be obtained:

$$\frac{\dot{\epsilon}_1}{\dot{\epsilon}_2} = \left(\frac{\sigma_1 - \sigma_t}{\sigma_2 - \sigma_t} \right)^m . \quad (7)$$

The values of σ_t for creep at 325 and 425 C and for 25 volume percent dispersoid MMCs at 225 C were determined by extrapolating the $\log \dot{\epsilon}$ vs. σ curves (Figs. 10, 11 and 12) to 90° slopes. Then m was determined from eq. (7). The results are given in Table 4. The m value for the 10 volume percent dispersoid MMCs is 3. This was assumed for 225 C creep and then σ_t was determined from eq. (7). These values are also given in Table 4 along with the previously reported values for m and σ_t of the 4 volume percent α -alumina and spinel dispersoids at 410 C by Creasy et al. (2).

The threshold stresses are obviously increased substantially by increasing the volume fraction of dispersoid. For the 10 volume percent dispersoid composites, the substantially larger σ_t with spinel is understandable on the basis of the 8 times smaller particle size (Table I). A moving

dislocation is more likely to encounter a particle for a given volume fraction and be trapped if the particle size is smaller. The unpinning stress (12), eq.(8),

$$\sigma_u = \frac{Gb}{2(1-v)L} \left(\frac{\pi^2}{12} + \ln \frac{r}{r_c} \right) \quad (8)$$

increases with particle size but interparticle spacing dominates. In eq.(8) L is the interparticle spacing and r is the particle radius while r_c is the dislocation core radius.

The threshold stresses for the 25 volume percent spinel and α -Al₂O₃ composites are not too different at the same temperature even though the α -Al₂O₃ particles are 4 times larger. It is suggested that most of the particles are at grain boundaries in both cases. Note that the grain sizes are almost equal (Table 2). Some spinel particles are inside grains but the alumina particles are larger. The interplay of these effects is suggested to give the observed behavior of nearly equal σ_t values.

The temperature dependence of the threshold stress is of interest. The only temperature dependent quantity in eq.(8) is G. The temperature dependence of the shear modulus is approximately -750 ppm/°K. This is much too small to account for the decrease in σ_t values between 225 and 425 K. A decrease of 200 C gives an increase in G of only 1.5%. Obviously, the temperature dependence of σ_t has another origin and possibly supports the relaxation factor approach of Artz and co-workers (11,13). Strong temperature dependence of σ_t has been correlated with small grain size through examination of a number of systems (14).

Conclusions

The mechanical properties of an aluminum + 3% magnesium matrix dispersion strengthened with either 10 or 25 oxide volume percent spinel or

α -alumina have been investigated as a function of strain rate and temperature. The creep resistance increases substantially with volume fraction of dispersoid at all temperatures investigated, 25 to 425 C. At all temperatures, the nominal 10 volume percent Al-spinel composite showed a 50% greater flow stress than the nominal 10 volume percent Al-alumina composite. Much of the strength difference is attributed to the smaller spinel particle size which reduces further during mechanical alloying than α -alumina. Conversely, the 25 oxide volume percent composites exhibit nearly identical strengths with varying particle size; however, the grain sizes are equal. The variation of flow stress with strain rate shows the presence of a threshold stress. Below a certain strain rate the flow stress is independent of strain rate. The threshold stress increases substantially with dispersoid content. It decreases considerably on heating to 425 C.

Extraction replicas of the Al-alumina composites exposed a reaction zone around α -alumina particles. The reduction of alumina by magnesium to form magnesium oxide and aluminum followed by the combination of magnesium oxide and alumina to form spinel has been shown to give a lowering in free energy.

References

1. H. G. F. Wilsdorf, Dispersion Strengthening of Aluminum Alloys, in Dispersion Strengthened Aluminum Alloys, Eds., Y.-W. Kim and W. M. Griffith, The Metallurgical Society, 1988.
2. T. Creasy, J. R. Weertman and M. E. Fine, Aluminum Alloy with Spinel For Oxide Dispersion Strengthening, in Dispersion Strengthened Aluminum Alloys, Eds. Y.-W. Kim and W. M. Griffith, The Metallurgical Society, 1988, pp. 539-549.
3. M. E. Fine, Dynamic Methods for Determining Elastic Constants and Their Temperature Variations in Metals, American Society for Testing Materials Tech. Publication No. 181, 1952, p. 20.
4. R. W. Hertzberg, Deformation and Fracture Mechanics of Engineering Materials, 3rd edition, John Wiley Pub., New York, 1989, p. 15.
5. M. E. Fine, Elastic Moduli of Two Phase Aluminum Alloys, Scripta Metall., 15, 1981, pp. 523-524.
6. C. M. Sellars and R. A. Petkovic-Luton, Creep of Dispersion-Strengthened Alloys, Mat. Sci. & Eng., 46, 1980, pp. 75-87.
7. G. M. Pharr and W. D. Nix, A Comparison of the Orowan Stress with the Threshold Stress for Creep for Ni-20Cr-2ThO₂ Single Crystals, Scripta Metall., 10, 1976, pp. 1007-1010.
8. R. S. Herrick, J. R. Weertman, R. Petkovic-Luton and M. J. Luton, Dislocation/Particle Interactions in an Oxide Dispersion Strengthened Alloy, Scripta Metall., 22, 1988, pp. 1879-1884.
9. D. Hull and D. J. Bacon, Introduction to Dislocations, 3rd edition, Pergamon Press, Oxford, 1984.
10. K. L. Murty, F. A. Mohamed and J. E. Dorn, Viscous Glide, Dislocation Climb and Newtonian Viscous Deformation Mechanisms of High Temperature Creep in Al-3Mg, Acta Metall., 20, 1972, pp. 1009-1018.
11. E. Artz and S. Wilkinson, Threshold Stresses for Dislocation Climb over Hard Particles: The Effect of an Attractive Interaction, Acta Metall., 34, No. 10, 1986, pp. 1893-1898.
12. D. J. Srolovitz, R. H. Petkovic-Luton and M. J. Luton, Diffusional Relaxation of the Dislocation-Inclusion Repulsion, Phil. Mag., 48A, 1983, pp. 795-809.
13. J. Rosler and E. Artz, A New Model-Based Creep Equation for Dispersion Strengthened Materials, Acta Met. et Mat., 38, 1990, pp. 671-683.
14. K. Tsuchiya, J. R. Weertman and M. J. Luton, Creep Threshold Behavior of a Fine-Grained Aluminum Alloy Produced by Cryomilling in Low Density High Temperature Powder Metallurgy Alloys, W. E. Frazier, M. J. Koczak & P. W. Lee, eds., The Minerals, Metals & Materials Soc., Warrendale, PA, 1991, pp. 251-266.

Table 1. Microstructural Characteristics of Al-alumina and Al-spinel Dispersion Strengthened Composites.

Material	Nominal Volume Percent	Actual Volume Percent	Initial Dispersoid Particle Size (μm) [*]	Final Dispersoid Particle Size (μm)
Al- 10 alumina	10	11 \pm 1.9	1.0	0.35 \pm 0.13
Al- 10 spinel	10	14 \pm 1.6	3.0	0.042 \pm 0.019
Al- 25 alumina	25	26 \pm 3.5	0.2	0.14 \pm 0.055
Al- 25 spinel	25	28 \pm 0.7	3.0	0.035 \pm 0.016

* from supplier

Numbers after \pm are standard deviations.

Table 2. Average Grain Sizes of Al-alumina and Al-spinel Composites

Material	Grain Size Longitudinal (μm)	Grain Size Transverse (μm)
Al- 10 alumina	0.96 \pm 0.032	0.77 \pm 0.26
Al- 10 spinel	0.68 \pm 0.30	0.35 \pm 0.15
Al- 25 alumina	0.30 \pm 0.15	0.24 \pm 0.11
Al- 25 spinel	0.30 \pm 0.19	0.22 \pm 0.10

Numbers after \pm are standard deviations.

Table 3. Ratio of Experimentally Determined CTE to Linear Law of Mixtures Prediction.

Material	Actual Oxide Volume Percent	Measured CTE ($\mu\text{m}/\text{m}^\circ\text{K}$)	Predicted CTE ($\mu\text{m}/\text{m}^\circ\text{K}$)	CTE ^M ;CTE ^P
Al- 10 alumina	11	23.8 \pm 0.4	25.0	0.96
Al- 10 spinel	14	24.4 \pm 0.31	24.3	1.00
Al- 25 alumina	26	20.3 \pm 0.6	22.0	0.92
Al- 25 spinel	28	21.3 \pm 0.9	21.3	1.00

Numbers after \pm are standard deviations.

Table 4. Threshold Stresses and Creep Exponents for α -Alumina and Spinel Dispersoids in Al-3% Mg Matrix Composites.

	225 C		325 C		410 C		425 C	
	σ_t (MPa)	m	σ_t (MPa)	m	σ_t (MPa)	m	σ_t (MPa)	m
4 v/o Al_2O_3 (2)					9	7		
10 v/o Al_2O_3	89	(3)*	77	3			40	3
25 v/o Al_2O_3	260	4	190	5			110	5
4 v/o spinel (2)					14	6		
10 v/o spinel	152	(3)*	147	3			81	3
25 v/o spinel	280	4	200	5			110	6

* assumed

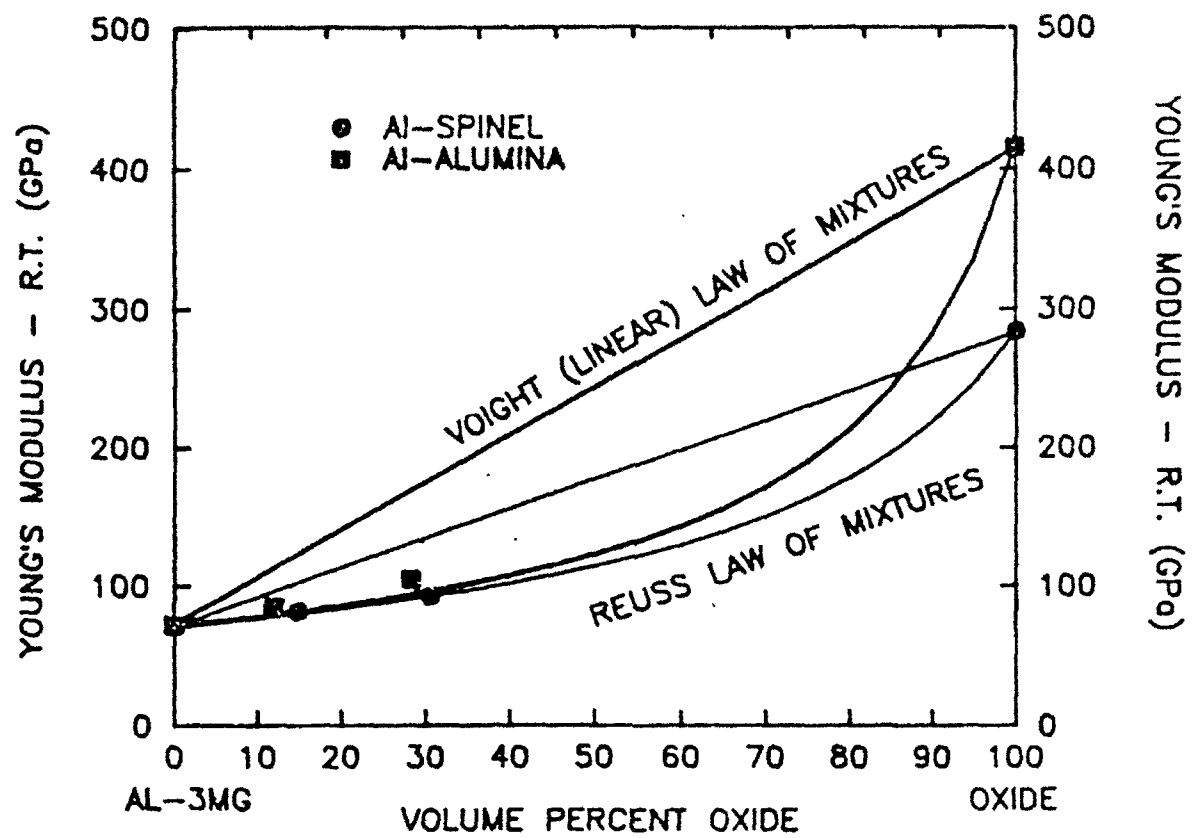


Figure 1 Elastic modulus of Al-alumina and Al-spinel composites as a function of oxide volume percent and Reuss and Voight laws of mixture.

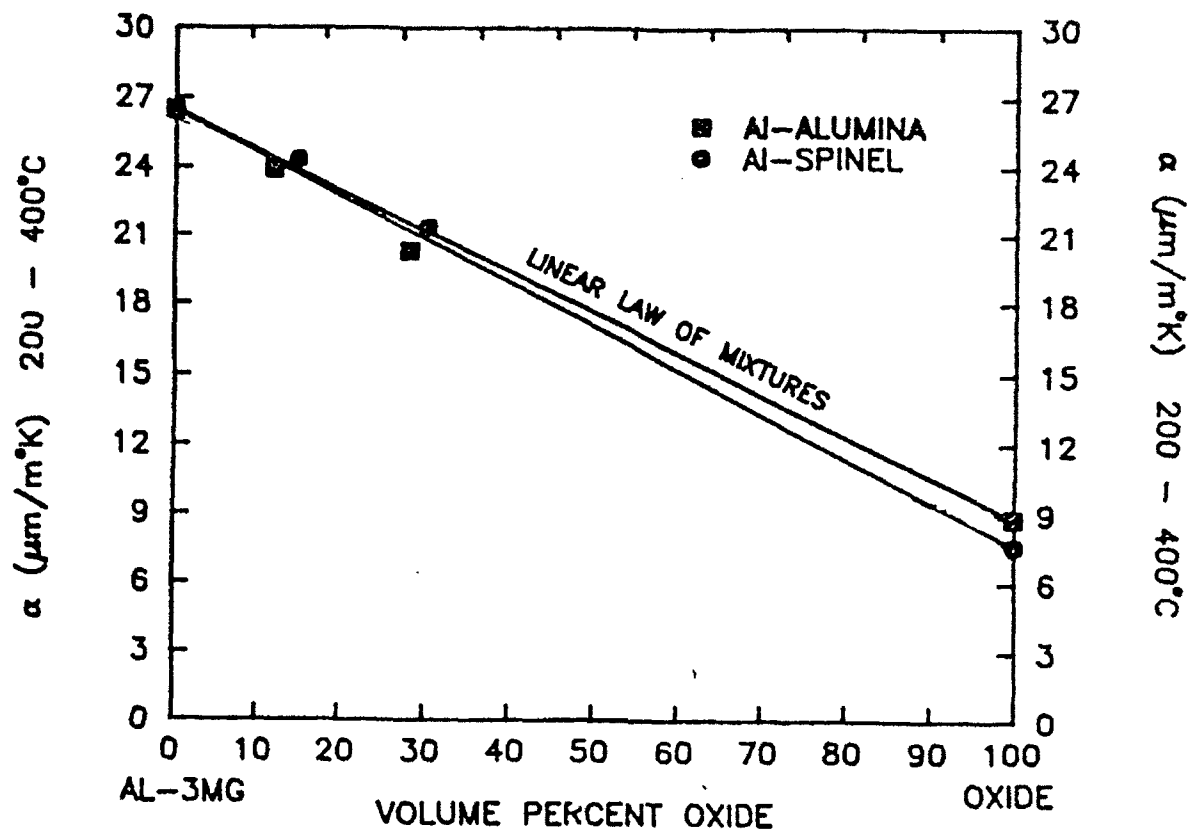


Figure 2 Coefficients of thermal expansion as a function of oxide volume percent and corresponding linear laws of mixture.

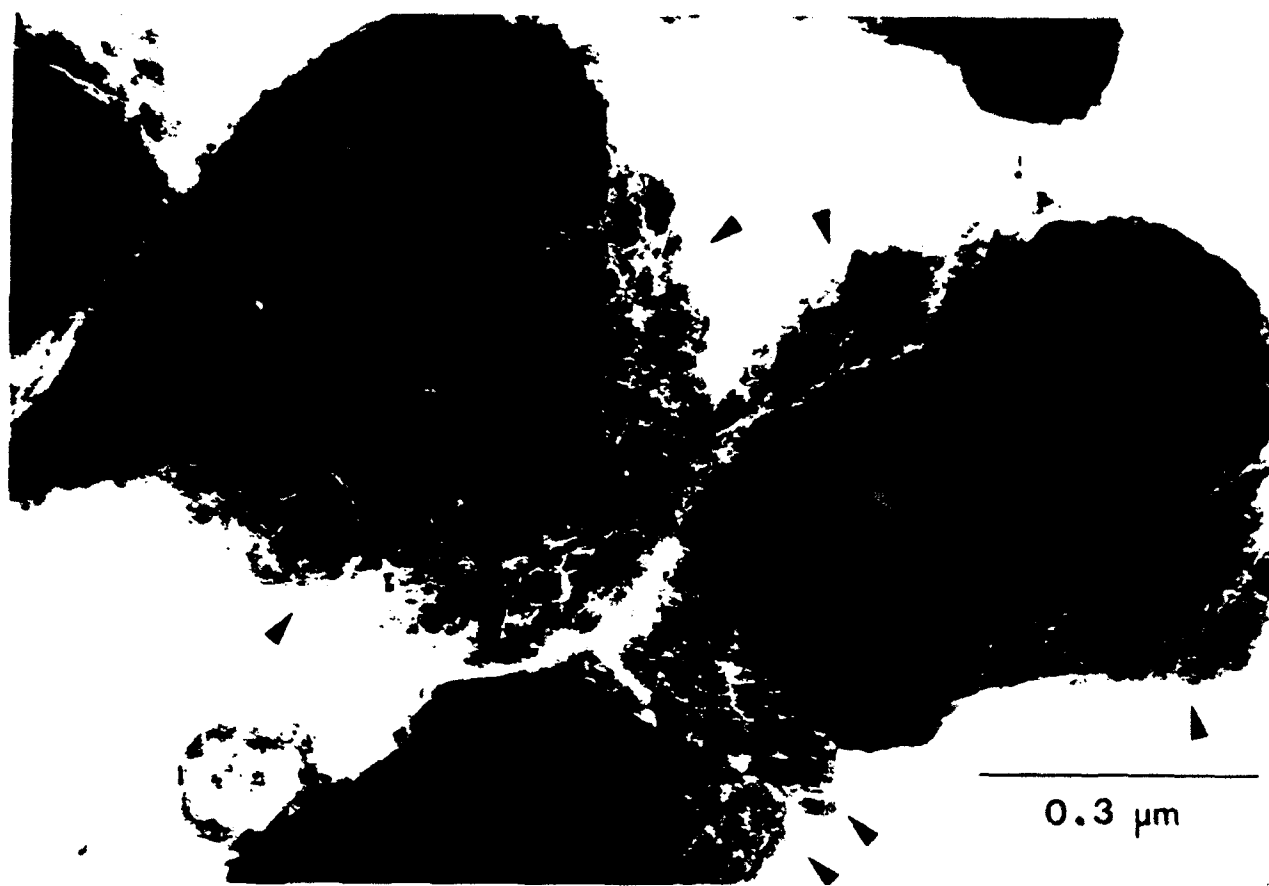
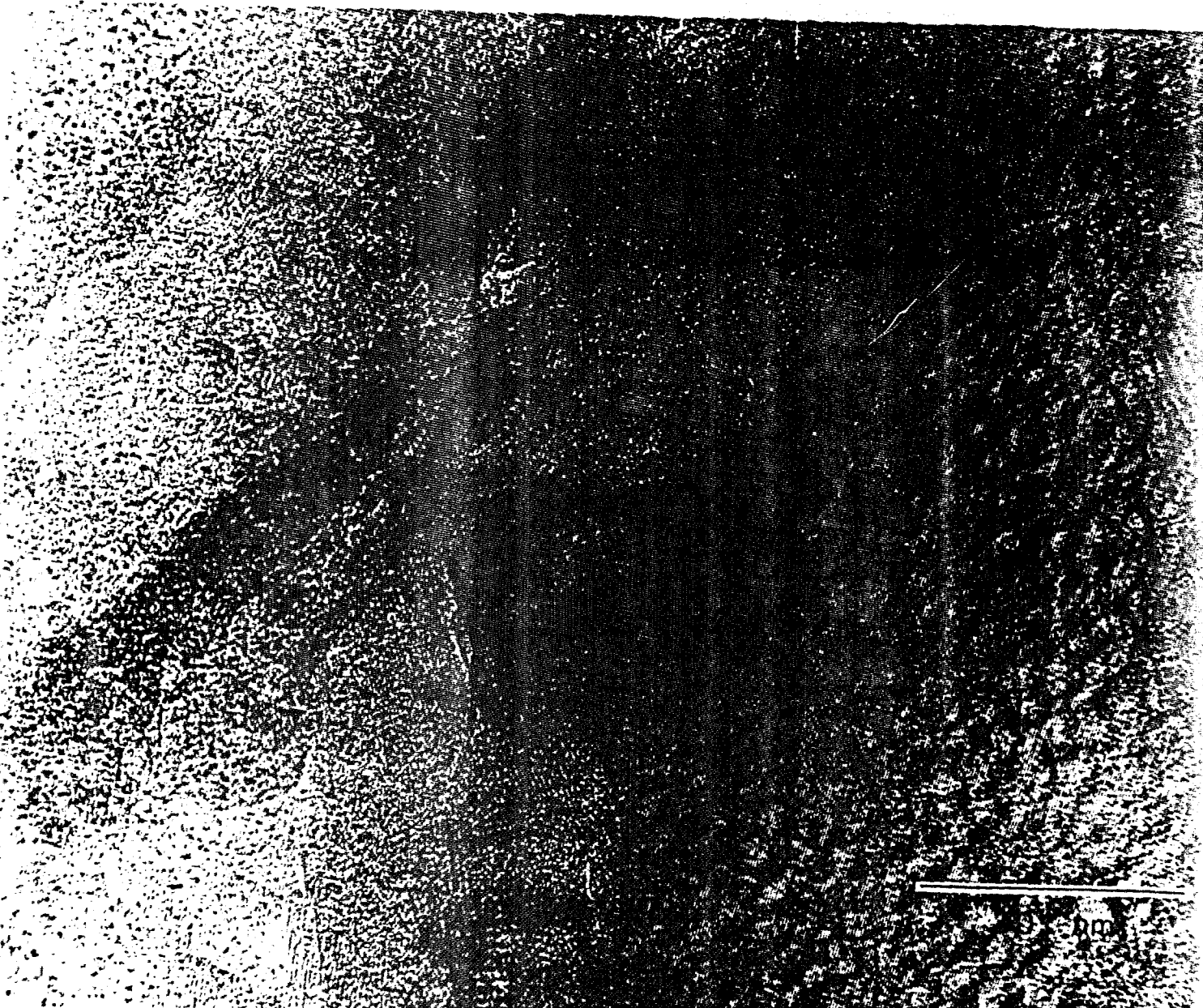


Figure 3 Extraction replica showing multicrystalline reaction zone around alumina particles in the as fabricated Al-10 volume percent alumina composite.



Figure 4 Conventional TEM micrograph showing a reaction zone around alumina particles (a,b,c) in the Al- 10 volume percent alumina composite.





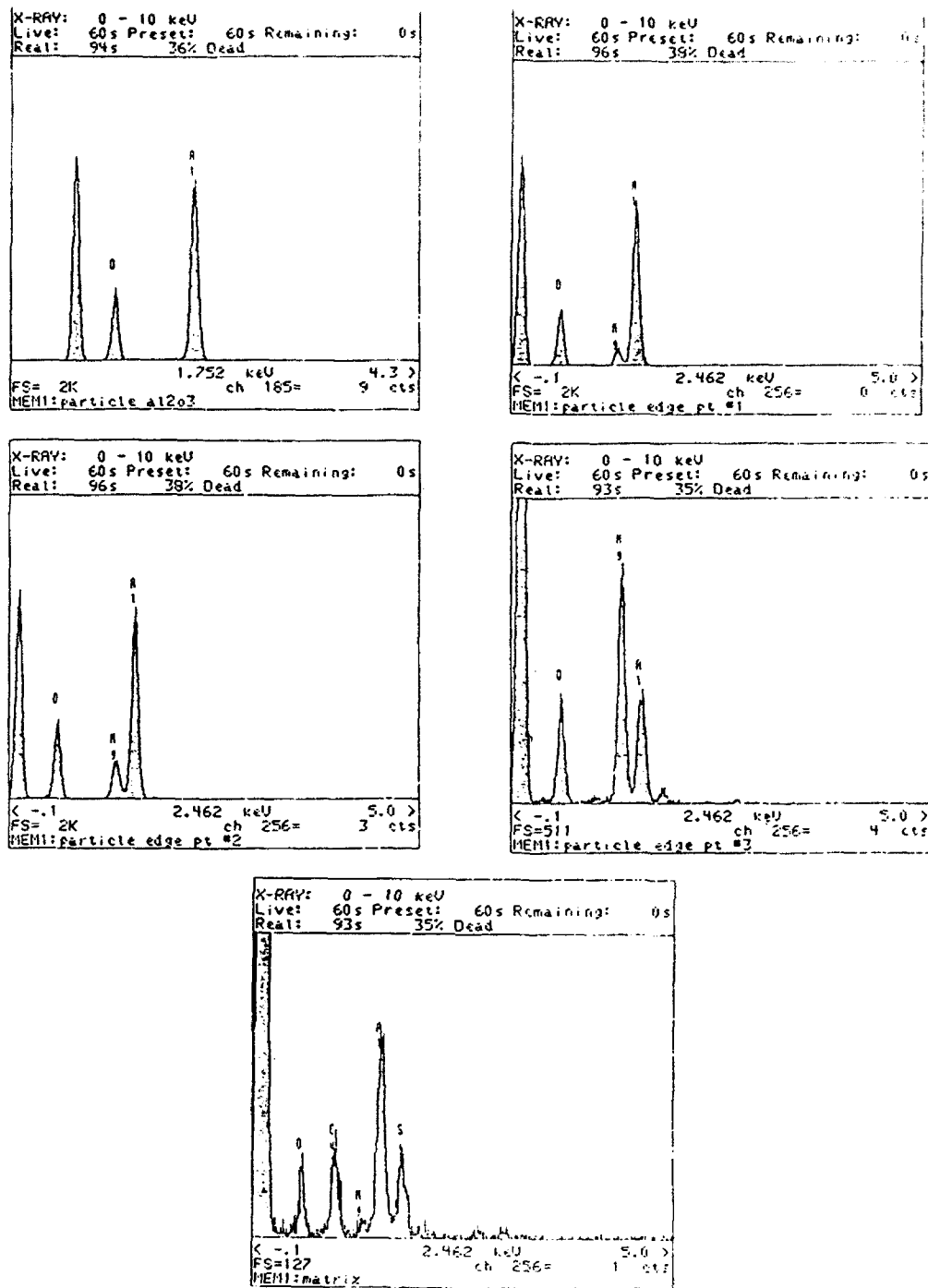


Figure 7 X-ray point spectra from five spots across the reaction zone: a) at the α -alumina particle b) at the α -alumina/reaction zone interface c) in the middle of the reaction zone d) at the reaction zone/matrix interface and e) in the matrix.

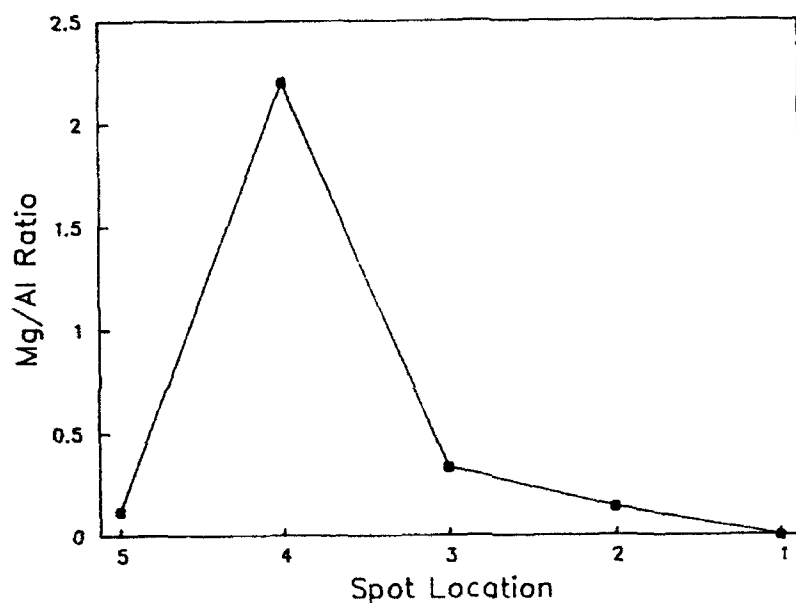
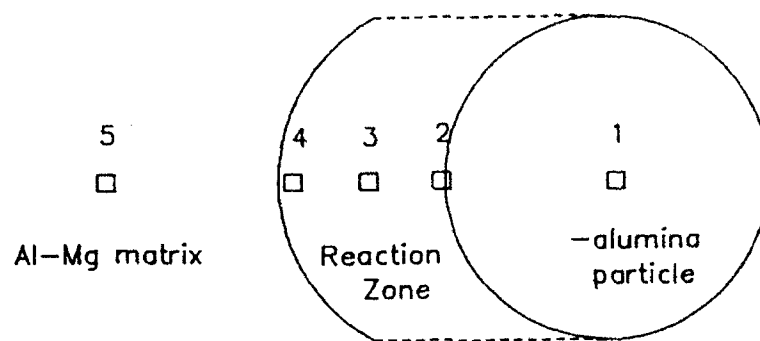


Figure 8 Schematic diagram showing the location of the five point x-ray analysis shown in figure 7 and the magnesium concentrations as determined by the area under the magnesium peaks.

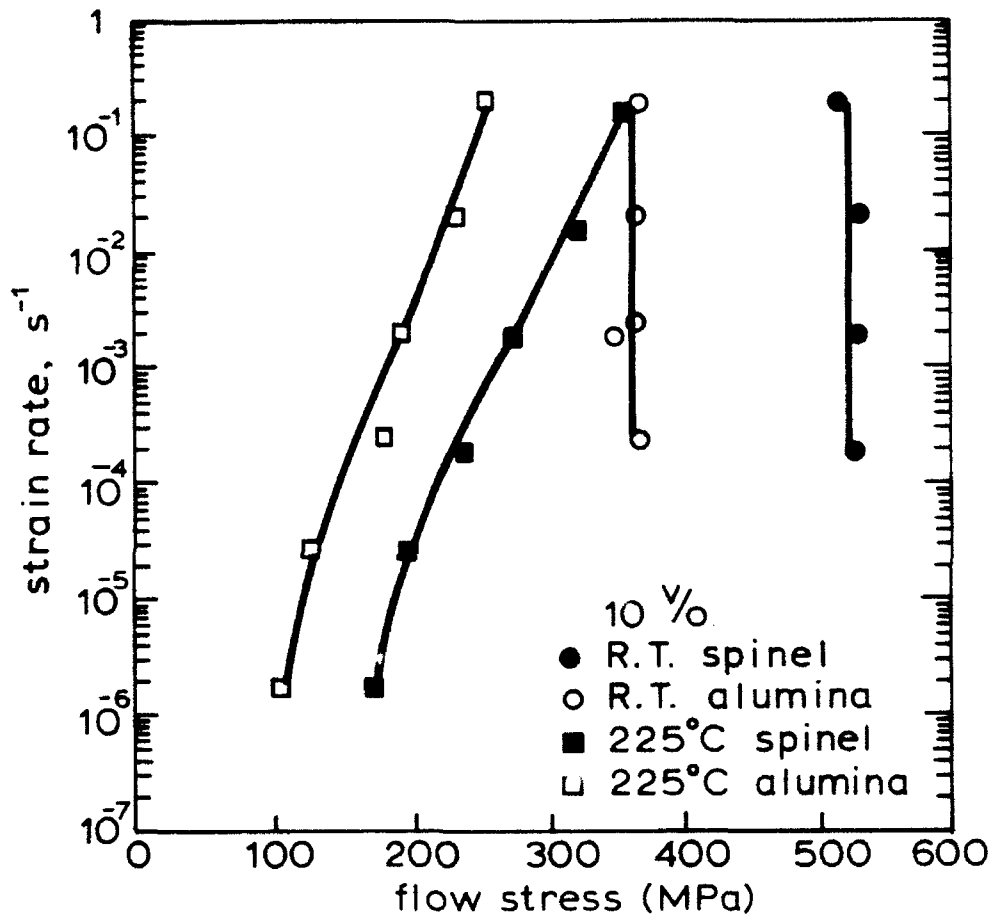


Figure 9 Compressive flow stresses of Al(3% Mg) - 10 volume percent alumina and Al- 10 volume percent spinel composites at room temperature and 225°C as a function of strain rate.

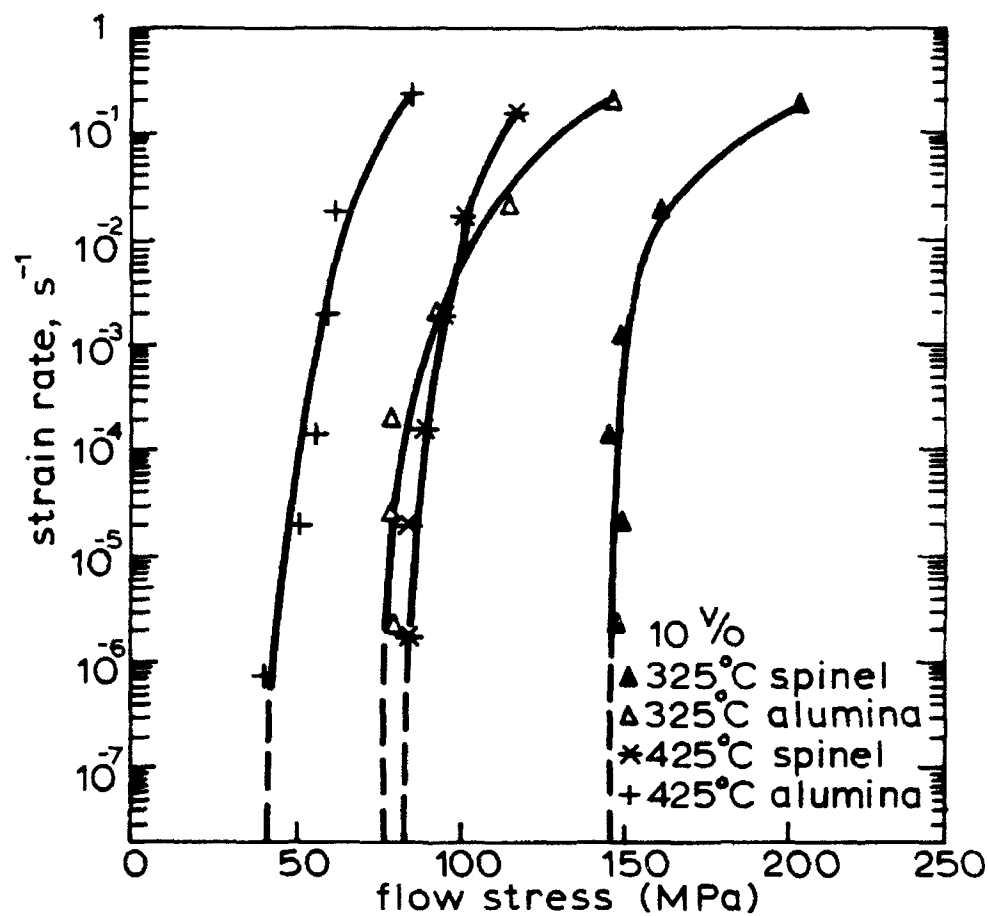


Figure 10 Compressive flow stresses of Al(3% Mg) - 10 volume percent alumina and Al- 10 volume percent spinel composites at 325 and 425 C as a function of strain rate.

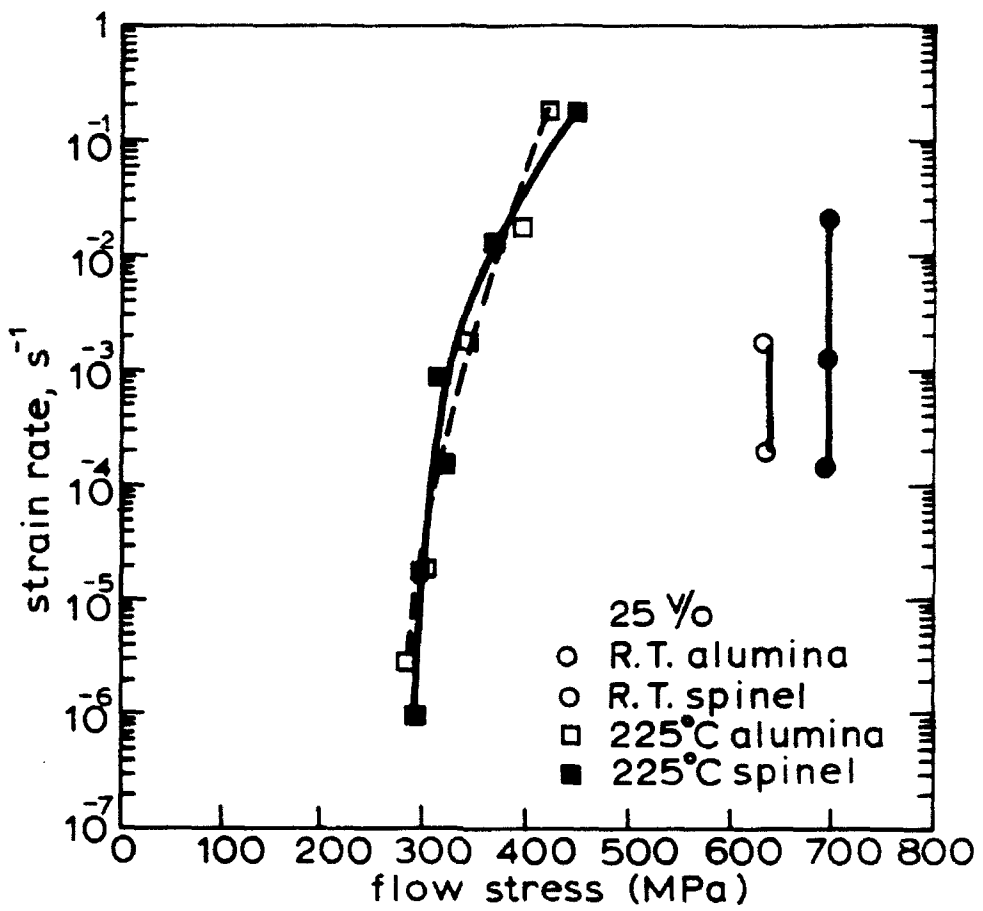


Figure 11 Compressive flow stresses of Al(3% Mg) - 25 volume percent alumina and Al- 25 volume percent spinel composites at room temperature and 225°C as a function of strain rate.

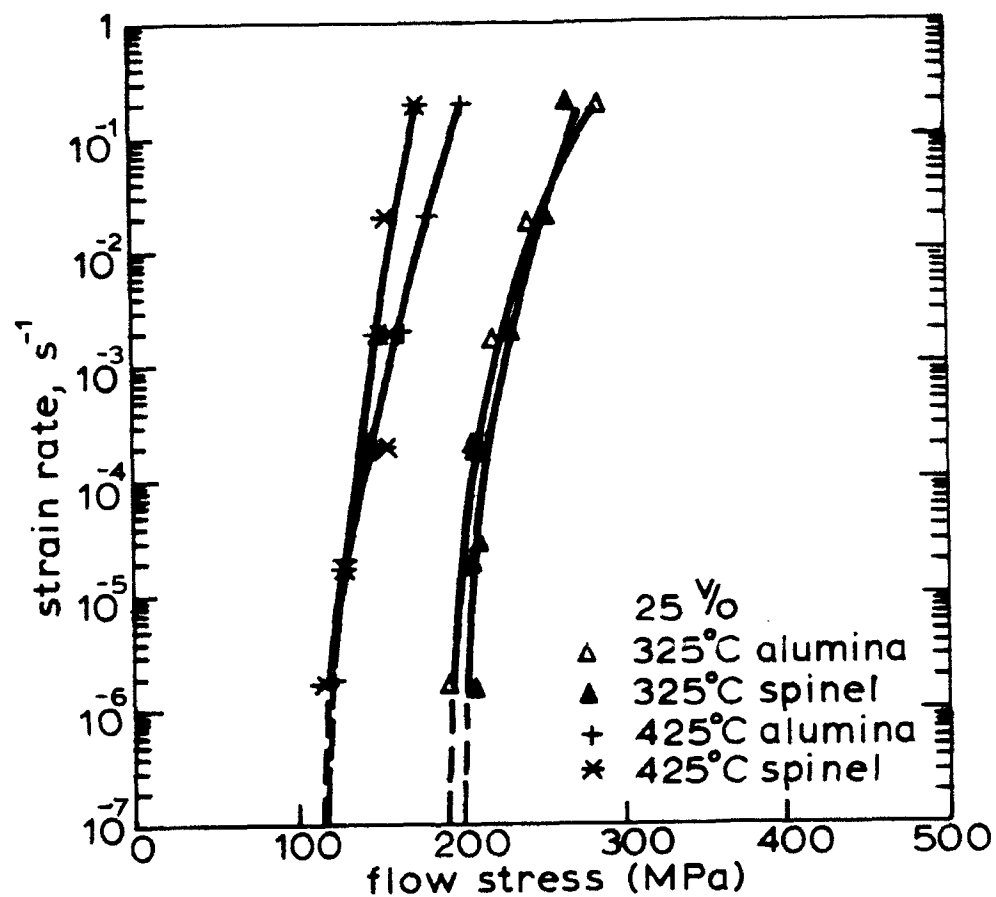


Figure 12 Compressive flow stresses of Al(3% Mg) - 25 volume percent alumina and Al- 25 volume percent spinel composites at 325 and 425°C as a function of strain rate.

II. Magnesium Metal Matrix Composites

by Neil R. Brown

This report summarizes the research results on magnesium metal matrix composites. The materials studied were particle reinforced magnesium alloy matrix metal matrix composites supplied by Dow Chemical Corporation. These composites have nominal compositions of :

Z6 (Mg, 6% Zn) / 20v% SiC extruded

EM31 (Mg, 3% Ce + La, 1% Mn) / 3v% SiC extruded

AZ91 (Mg, 9% Al, 1% Zn) / 10v% SiC cast

AZ91 (Mg, 9% Al, 1% Zn) / 5v% Al₂O₃ cast.

The composites were produced by a proprietary fluxless casting method in which the reinforcement is stirred into the melt followed by casting and possible extrusion¹. The thrust of the research was on the effects of interfacial reaction zones on composite mechanical properties.

Reaction Zone Determination

Samples were held at 773 K in an argon atmosphere for periods of time up to 192 hours to allow for a sizable reaction zone to form. The extent and composition of the composites' reaction zones were determined using transmission electron microscopy, selected area diffraction and scanning transmission EDAX.

Z6 / SiC

The as received Z6 / SiC matrix was overaged during hot extrusion. Large

incoherent β MgZn intermetallics are observed in the as received matrix, Fig. (1.a).

After 1 hour at 773 K, followed by rapid cooling, coherent β' MgZn intermetallics are present, Fig. (1.b). This change in matrix microstructure coincides with changes in the composite mechanical properties discussed subsequently. The as received Z6 / SiC composite interface was free of interfacial reaction zone with some preferential nucleation of MgZn intermetallic present, Fig. (1.c). After 192 hours at 773K, a reaction zone of Mg_2Si is present, Fig. (1.d). The reaction equation for Mg and SiC at 773K:



predicts a slight reaction since the free energy of formation is low². Carbon is expected in the reaction zone since magnesium does not form a carbide (except when magnesium powder is reacted with a hydrocarbon near the melting point³). Carbon was not observed in the reaction zone, since EDAX cannot detect carbon and the amorphous carbon is a poor electron diffractor.

EM31 / SiC

The EM31 / SiC as received interface was free of interfacial reaction products, with some preferential precipitation of Mg_12Ce intermetallic, Fig (2.a). After 192 hours at 773 K, an extensive reaction zone of Mg_2Si and Ce_2C_3 formed, Fig. (2.b). This is in accordance with the reaction equation:

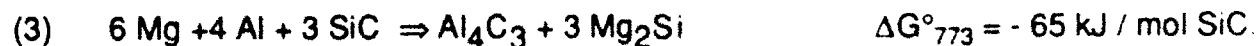


Note that the addition of Ce to the matrix allows for formation of a carbide, significantly increasing the change in free energy of formation over a pure magnesium / SiC

reaction. No noticeable change in matrix microstructure was observed, although the interfacial reaction consumes Ce from the matrix.

AZ91 / SiC

The interfaces of the AZ91 / SiC composites were free of interfacial reaction zones and no preferential precipitation of intermetallics was observed, Fig. (3.a). After 192 hours at 773 K a reaction zone of Mg_2Si and Al_4C_3 was observed, Fig. (3.b). This is in accordance with the reaction equation:



Note that the addition of aluminum to the matrix increases the change in free energy of reaction zone formation over a pure magnesium matrix. No change in matrix microstructure was observed, although Al is consumed during the interfacial reaction.

AZ91 / Al₂O₃

The AZ91 / Al₂O₃ interface was found to be free of preferential precipitation of intermetallics and reaction zones in both the as received and after 192 hours at 773 K, Fig. (4). This is in contrast to the reaction equations for this interface:



The above equations, however, do not account for the reaction kinetics, which have been shown to be quite slow, due to the slow diffusion of aluminum through the reaction zone layers of MgO and MgAl₂O₄^{4,5}. Several researchers have observed reaction zones between magnesium and alumina fibers, however, the alumina fibers

contain SiO_2 as a binder that magnesium readily reduces².

Work of Adhesion and Interfacial Energy

The work of adhesion is the energy necessary to separate a unit area of interface and is described by:

$$(5) \quad W_{ad} = \gamma_{pv} + \gamma_{mv} - \gamma_{pm}$$

where γ_{pv} is the particle surface energy, γ_{mv} is the matrix surface energy, and γ_{pm} is the interfacial energy of the particle and matrix. From Eq. (5) it is clear that a low interfacial energy results in a high work of adhesion. The interfacial energy can be determined from the contact angle of an interfacial void in equilibrium through Young's equation⁶ knowing γ_{mv} and γ_{pv} :

$$(6) \quad \gamma_{pm} = \gamma_{mv} \cos \theta + \gamma_{pv}$$

where the contact angle θ is the tangential contact angle between the matrix and the interfacial void, Fig. (5). By substituting Eq. (6) into Eq.(5) the work of adhesion can also be determined from the void / particle contact angle:

$$(7) \quad W_{ad} = \gamma_{mv} (1 - \cos \theta)$$

where the work of adhesion can now be determined without knowledge of the interfacial energy or particle surface energy.

As received composites and samples thermally exposed to 773 K for 192 h were cold rolled to a reduction in thickness of 25% followed by annealing at 773 K for one hour to ensure equilibrium conditions. The surfaces were then polished and the void / particle contact angles measured. The average contact angle in the AZ91 / Al_2O_3 composite was $70^\circ \pm 5^\circ$ for the two conditions, indicating no change in the interface

due to thermal exposure. The average void particle contact angle in the SiC reinforced material decreased from $60^\circ \pm 5^\circ$ in the as received condition to $10^\circ \pm 3^\circ$ in the composite exposed for 192 h at 773 K, Fig(6), indicating a large decrease in the work of adhesion with reaction zone formation. In the severely exposed SiC reinforced samples, the interfacial debonding occurred between the reaction zone and the SiC. Furthermore, the number of SiC particle interfaces containing voids increased from 5% to 30 % with reaction zone formation. The interfacial energies and work of adhesion were then calculated using Eqs. (6,7) and are summarized in Table 1. The surface energy values were taken to be: Mg = 556 mJ / m², SiC = 1207 mJ / m², Al₂O₃ = 905 mJ / m² and Mg₂Si = 2020 mJ / m².

Mechanical Properties

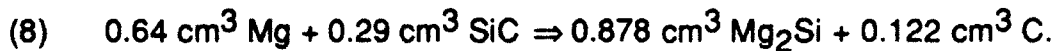
Young's Modulus

The room temperature Young's modulus of the composites were determined as a function of time at 773 K. The modulus was determined by a non destructive resonant frequency technique described previously⁷. The initial modulus of the composites falls within the theoretical bounds provided by Hashin and Shtrikman⁸, Fig. (7). The modulus results versus time at 773 K are summarized in Fig. (8). The SiC reinforced composites exhibit a significant degradation with increasing exposure, while little change is noted in the AZ91 / Al₂O₃ composite where no reaction zone is observed.

Since the composites contain differing volume fractions of reinforcement phases, direct comparison on the effects of reaction zone formation on mechanical properties is difficult. As a first order approximation, the change in modulus, normalized by volume fraction is plotted in Fig. (9). After normalization the adverse effects of aluminum and cerium are quite evident, with much higher decreases in normalized

modulus observed for the EM31 / SiC and AZ91 / SiC composites compared to the Z6 / SiC composite.

The effects of reaction zone formation were modeled to determine if third phase formation, due to interfacial reaction, was sufficient to cause the observed decreases in Young's modulus. The reaction zone of the Z6 / SiC composite was expected to have the lowest modulus consisting of Mg_2Si and C and was thus chosen to establish the maximum decrease in modulus due to third phase formation. Using the lower limit of the Hashin and Shtrikman bounds the modulus of the reaction zone was estimated to have a lower limit of 55 GPa. Next the constituent volume fractions were determined for a given amount of reaction zone formation by converting the reaction zone formation equation, Eq. (1) from molar quantities to volumes:



For the calculations the initial quantities were assumed to be $800 \text{ cm}^3 \text{ Mg}$ and $200 \text{ cm}^3 \text{ SiC}$ for the Z6 / SiC composite.

Since the theories for composite modulus do not readily handle more than two phases, the modulus of the reaction product coated particles was estimated and then returned to the matrix, in the proper quantities, and the new composite modulus was then determined. The above procedure was applied for Halpin and Tsai equations⁹, Hashin and Shtrikman upper and lower bounds⁸, and the isostress and isostrain theories. The results are presented in Fig. (10) along with the experimentally observed changes in modulus and estimated percentage of reaction zone formation from TEM observations. Clearly, the expected changes in modulus due to third phase formation cannot account for the observed decreases.

Another mechanism to account for the changes in Young's modulus is the

formation of microcracks along the particle matrix interface. With knowledge of the modulus drop and an assumed crack geometry the nondimensional crack density parameter, β , necessary to cause the observed change in modulus can be determined:

$$(9) \quad E/E_0 = 1 - k\beta$$

where E is the modulus of the cracked material, E_0 the initial modulus, k is a geometric term describing the crack shape and $b = N \langle a^3 \rangle$ for penny shaped cracks with $\langle a \rangle$ the average crack radius. N is the number of cracks per unit volume¹⁰. The k value for an array of three dimensionally randomly oriented penny shaped cracks, 2.282, was used. If the cracks are assumed to occur at the particle matrix interface and assumed to be about the same size as the particle facets, a fraction of the total interface area that is debonded can be estimated from a knowledge of β , average particle size, number of facets per particle, and particle density. Results are given in Table 2. This procedure overestimates the crack density, since the material is assumed to be homogeneous in the calculation. With cracking occurring along the particle matrix interface, the cracks will lower the modulus of the composite more than predicted because the microcracking theory does not take into account the debonding of the particles that would occur along with interface cracking.

To determine the presence and nature of interface cracking, the EM31/SiC after 192 h at 773 K was strained in tension to ≈ 0.25 the yield stress, surface replicas were taken and then examined in the SEM after shadowing. The majority of the particle interfaces exhibited cracking, Fig (11). From the replica results, it is unclear as to

whether cracking occurred between the matrix and the reaction zone or the reaction zone and the SiC.

Thermal stresses could be responsible for the microcracking at the interface. Since the reaction zone forms at 773 K, upon cooling to room temperature large stresses are expected due to thermal mismatch between the reaction zone and the SiC particles. Samples in both the as received condition and after 192 h at 773 K were thermally cycled from room temperature to 77 K (liquid nitrogen) and their room temperature modulus determined. The results are shown in Fig (12). Clearly the samples with reaction zones exhibited larger decreases in modulus due to thermal cycling than the reaction free samples.

Tensile Properties

The room temperature mechanical properties of the Z6 / SiC and EM31 / SiC composites were adversely affected by exposure to 773 K due to formation of reaction zones. These properties included the yield stress, ultimate tensile strength and strain to failure. The results are summarized in Fig. (13) and Fig. (14). The nature of the fracture surfaces changed from ductile failure with tear ridges in the as received samples to brittle failure accompanied by particle pullout upon reaction zone formation, indicating a brittle interface, Fig. (15).

Conclusions

The SiC reinforced composites exhibited extensive reaction zone formation after 192 h at 773 K. Furthermore, the Al and Ce used in the AZ91 and EM31 matrices, respectively, increased the interfacial reactions through formation of aluminum and cerium carbides. No reaction zone was observed in the AZ91 / Al_2O_3 interface due to slow reaction kinetics. The interfacial energies and works of adhesion were determined for the composites with and without reaction zones. Reaction zone

formation dramatically decreased the energy necessary to create a void at the interface. The SiC reinforced composites exhibited large decreases in Young's modulus with reaction zone formation that could not be accounted for solely by the formation of a third phase. Interfacial debonding was noted and shown to easily account for the drop in Young's modulus. Finally, the room temperature tensile properties of the Z6 / SiC and EM31 / SiC composites were found to significantly deteriorate after thermal exposure at 773 K. Furthermore, the fracture mode changed from ductile with matrix tear ridges to brittle accompanied by particle pullout. Clearly the formation of reaction zones is detrimental to the mechanical properties of the composites.

References

1. Mikucki, B.A., S.O. Shook, W.E. Mercer, W .G. Green, W. G. in 43 Annual World Magnesium Conference, 15 - 18 June 1986 Los Angeles, California, (1986)
2. Barin, I. Thermochemical Data of Pure Substances; Vol.1,2 (Weinheim, Germany: VCH Verlagsgesellschaft mbH, D-6940, 1989)
3. Rueggeberg, W.H.C. "The Carbides of Magnesium" J. Amer. Cer. Soc. **65**, p. 602-607(1943)
4. Hallstedt, B., Z.K. Liu and J. Agren "Fibre - Matrix Interactions During Fabrication of Al_2O_3 - Mg Metal Matrix Composites" Mat. Sci. and Eng. A129, p. 135 - 145 (1990)
5. McLeod, A.D and C.M. Gabryel "Kinetics of the Growth of Spinel, $MgAl_2O_4$, on Alumina Particulate in Aluminum Alloys Containing Magnesium" Metall. Trans. **23A**, p. 1279 - 1283 (1992)
6. Young, T. Trans. R. Soc. **94**, p. 65 (1805)
7. Fine, M.E. "Dynamic Methods for Determining the Elastic Constants and Their Temperature Variation in Metals" ASTM Special Technical Publication, Symposium on Determination of Elastic Constants, (American Society for Testing Materials, Philadelphia, PA), ASTM STP 129, 43, (1952)
8. Hashin, Z. and S. Shtrikman "A Variational Approach to the Theory of the Elastic Behaviour of Multiphase Materials" J. Mech. Phys. Solids, **11**, p. 127 - 140, (1963)
9. Halpin, J.C. and J.L. Kardos " The Halpin-Tsai Equations: a review" Polymer Engineering and Science **16**, p. 344 - 352 (1976)
10. Budiansky, B. and R.J. O'Connell "Elastic Modului of a Cracked Solid" Int. J. Solids and Structures, **12**, p 81-97 (1976)

Table 1. Summary of work of adhesion and interfacial energy determined through Young's equation. Note that the work of adhesion appears independent of the matrix alloying elements.

Calculated Energies (mJ/m ²)		
<u>Material</u>		
Hours at 773 K	$\gamma_{mp}(\theta)$	$W_{ad}(\theta)$
<u>Z6/SiC</u>		
1	1500	300
192	2000	10
<u>EM31/SiC</u>		
1	1500	300
192	2000	10
<u>AZ91/SiC</u>		
1	1500	300
192	2000	10
<u>AZ91/Al₂O₃</u>		
1	1100	400
192	1100	400

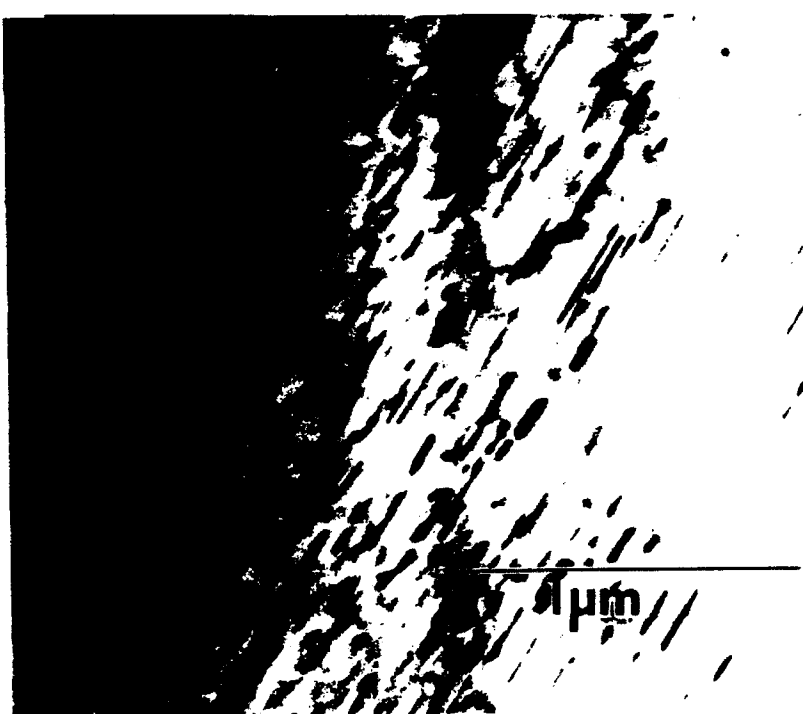
Table 2 Crack densities necessary to account for observed decrease in Young's modulus. If the cracks are assumed to be along the reaction zone, the percentage of cracked interface can be estimated. This estimate is too large, however, since the microcracking theory does not account for particle debonding caused by interface cracking.

Reaction Zone (% SiC reacted)	E / E_0	Nondimensional Crack Density, β	Percent of Interface Cracking
Z6 / SiC 11.	0.934	0.0289	7.9
EM31 / SiC 25.	0.914	0.0377	69
AZ91 / SiC 20.	0.904	0.0420	23

Figures



(a)



(b)



(c)



(d)

Fig.1 Transmission electron micrographs of Z6 / SiC composite, showing matrix microstructure and SiC interface. (a) As-received matrix, containing large incoherent MgZn precipitates; (b) after 1 hour at 773K, with needle-like coherent beta' MgZn precipitates; (c) Matrix / SiC interface after 1 hour at 773K, showing preferential precipitation of MgZn but no reaction zone; (d) interface after 192 hours at 773K showing extensive Mg₂Si reaction zone.

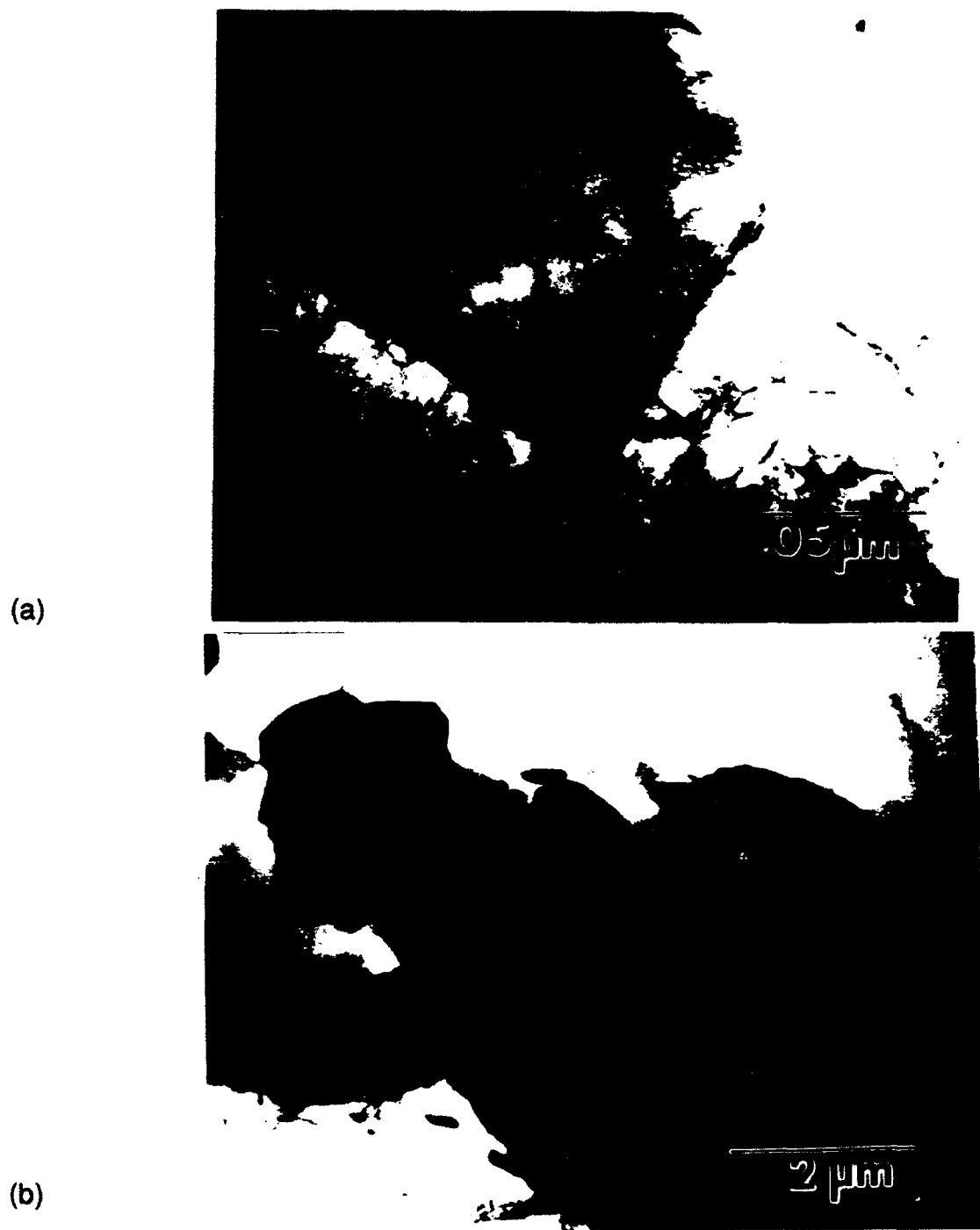
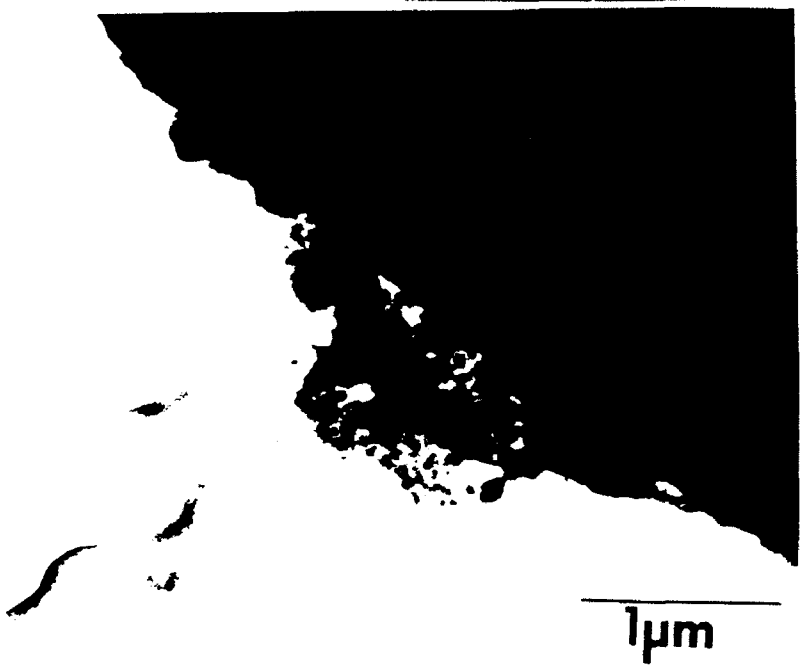


Fig. 2 TEM micrographs of EM31 / SiC composite. (a) As-received condition. Note evidence of preferential precipitation at the interface of the $Mg_{12}Ce$ intermetallic phase but an otherwise clean interface; (b) after 192 hours at 773K an extensive reaction zone of Ce_2C_3 and Mg_2Si has formed.



(a)



(b)

Fig. 3 TEM micrographs of AZ91 / SiC. (a) As-received condition. Note clean interface with absence of intermetallic precipitates; (b) interfacial reaction zone of Al_4C_3 and Mg_2Si after 192 hours at 773K.



Fig. 4 TEM micrograph of AZ91 / Al_2O_3 composite held at 773K for 192 hours. No reaction zone is visible. Contrast near interface is due to thickness contour.

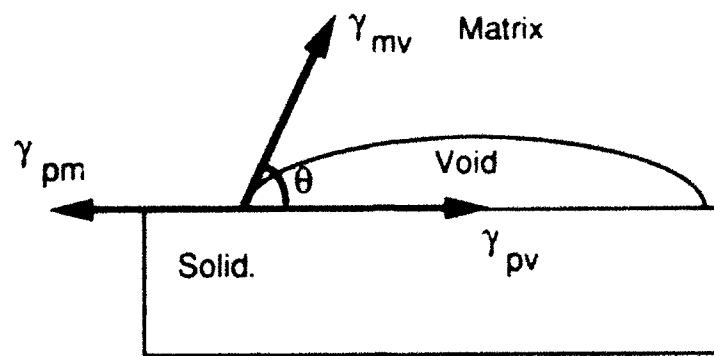


Fig. (5) Void / particle contact geometry used for determining interfacial energy and work of adhesion.

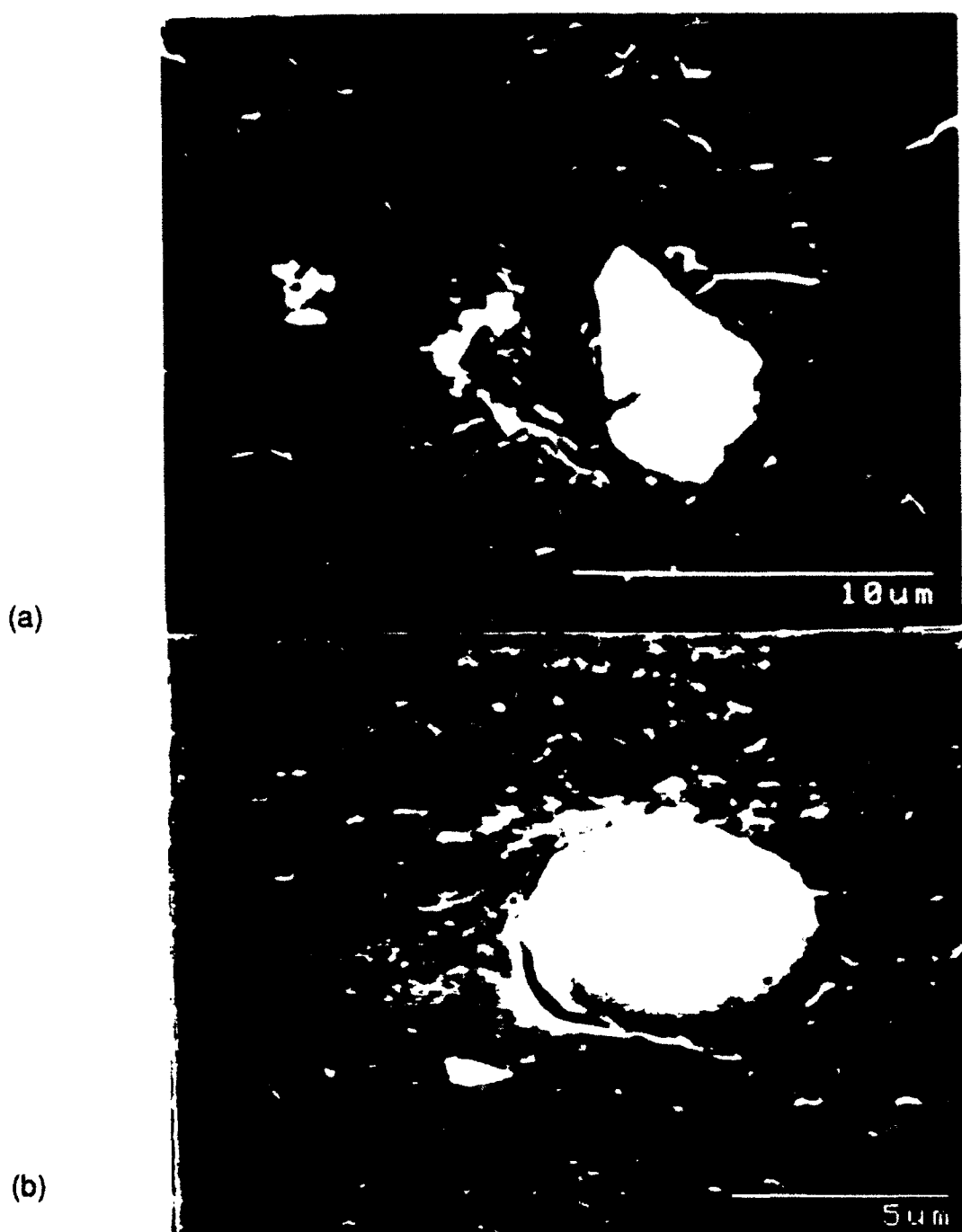


Fig. 6

Voids at Z6 / SiC particle matrix interface produced by cold rolling. (a) After 1 hour at 773 K; (b) after 192 hours at 773 K. Note the large decrease in void / particle contact angle with reaction zone formation.

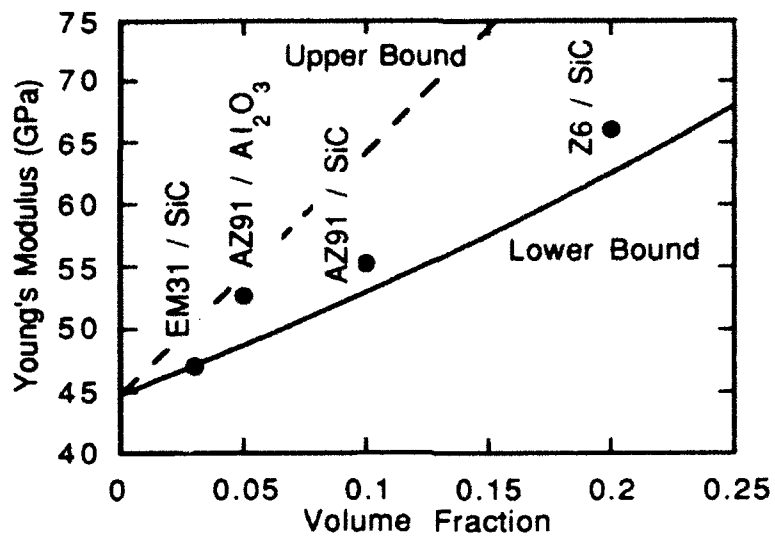


Fig. 7 Hashin and Shtrikman Upper and Lower Bounds of Young's modulus versus volume fraction of SiC particles. Experimental data of the as received composites is also plotted.

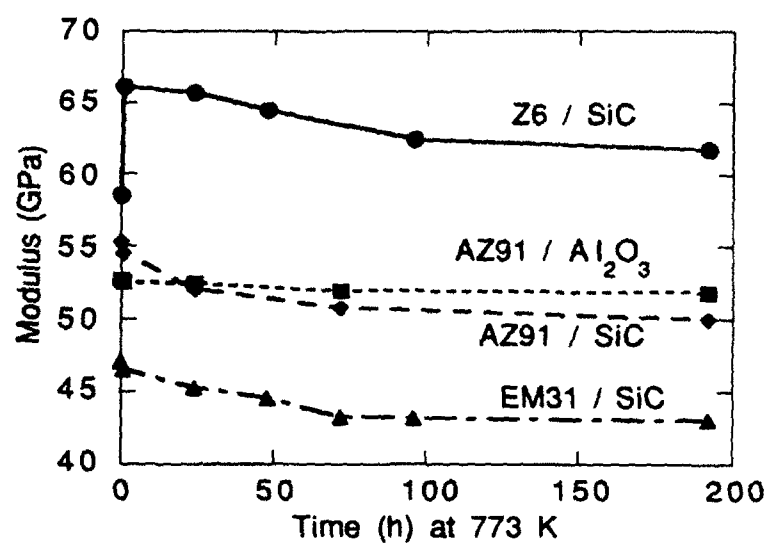


Fig. 8 Average room temperature Young's modulus versus time at 773 K.

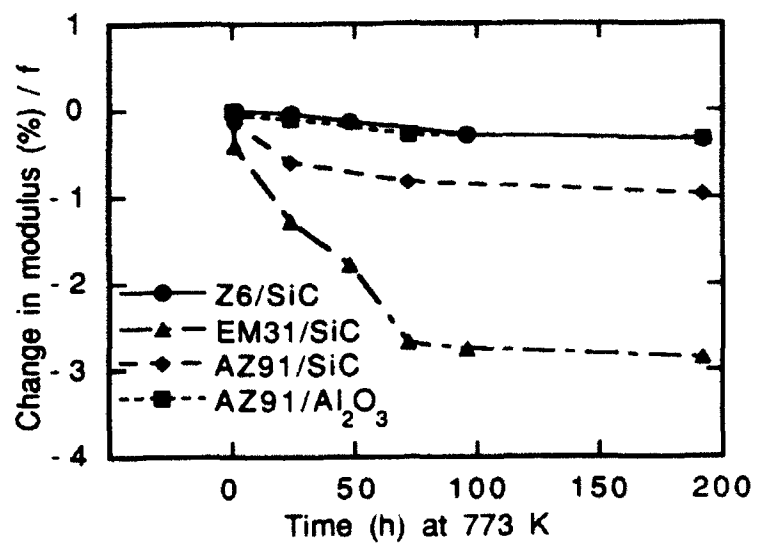


Fig. 9 Drop in elastic modulus normalized by particle volume fraction. Effect of alloying additions of Al and Ce is pronounced.

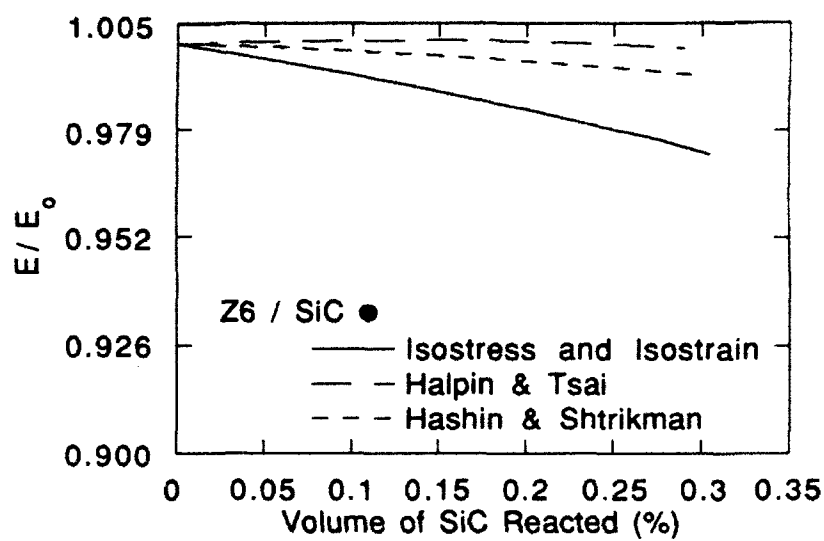


Fig. 10 Drop in modulus for Z6 / SiC 20 v% composite as a function of volume percent of SiC reacted. The drop in modulus cannot account for the observed decreases in modulus.

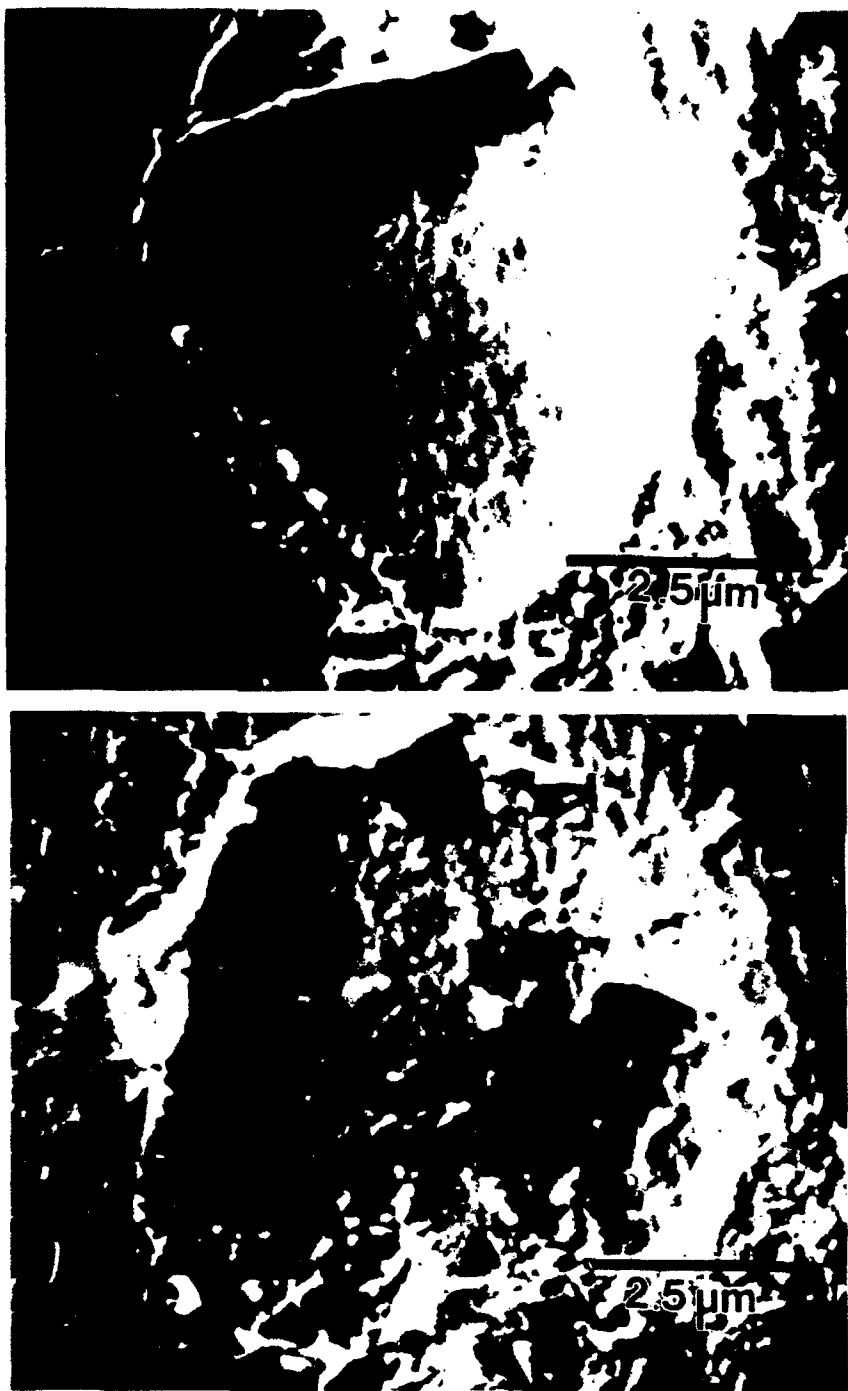
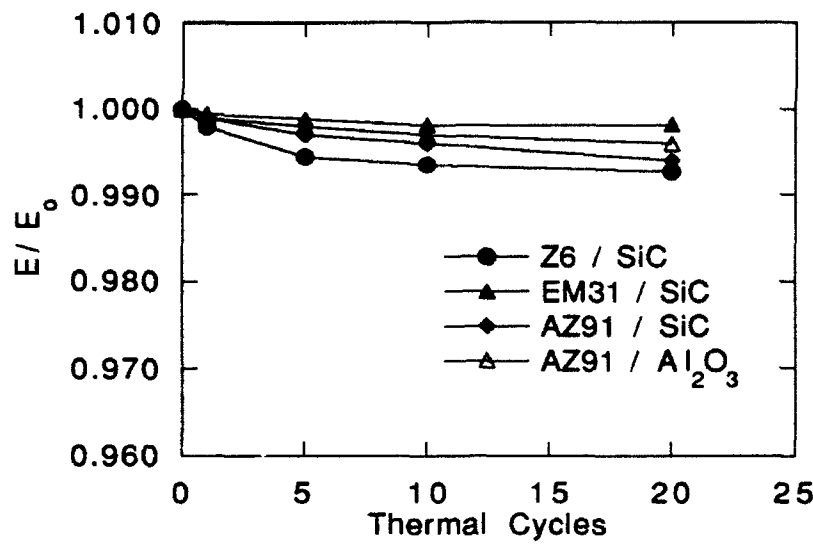
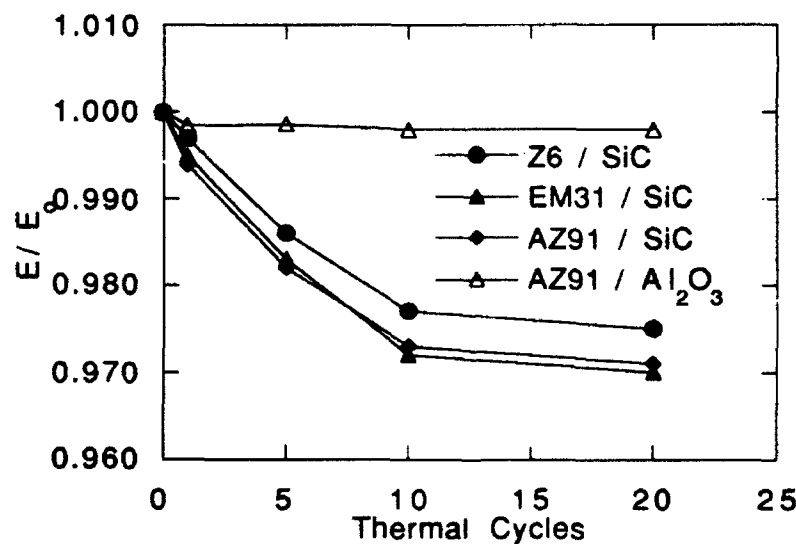


Fig. (11) SEM surface replicas of EM31 / SiC after 192 h at 773 K. Replication was done under 0.25 yield stress to open up the cracks. Cracking is noted parallel to the particle matrix interface.

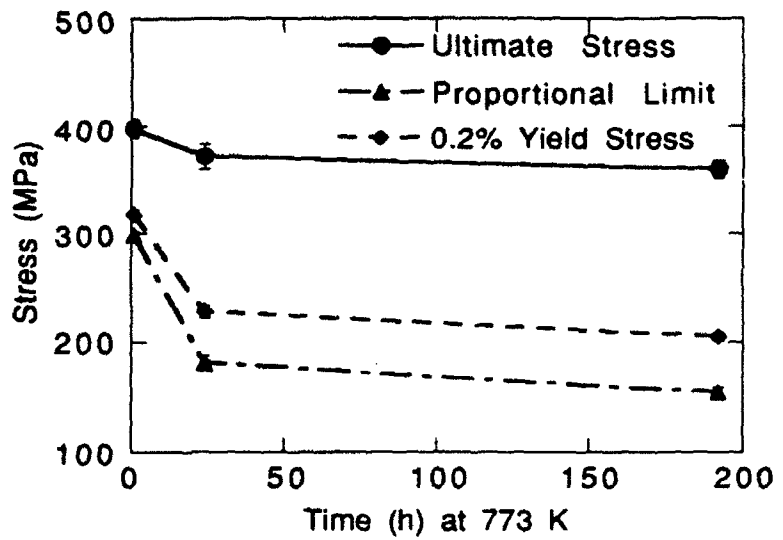


(a) 1 hour / 773K

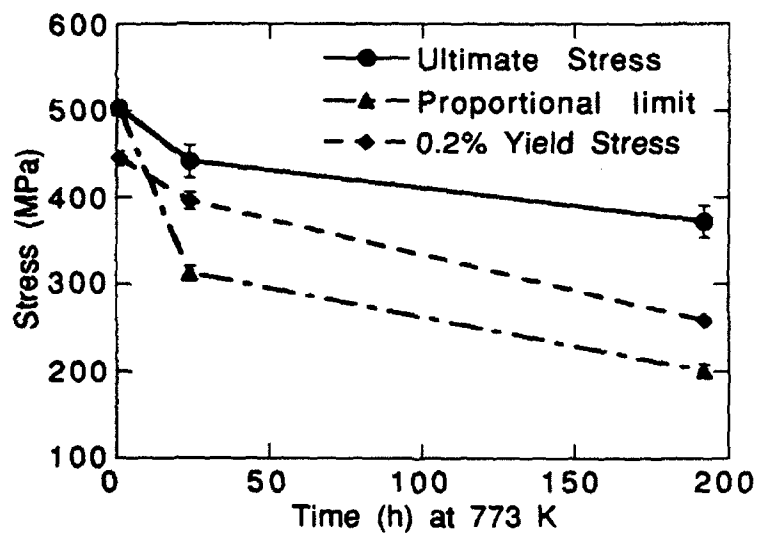


(b) 192 hours at 773K

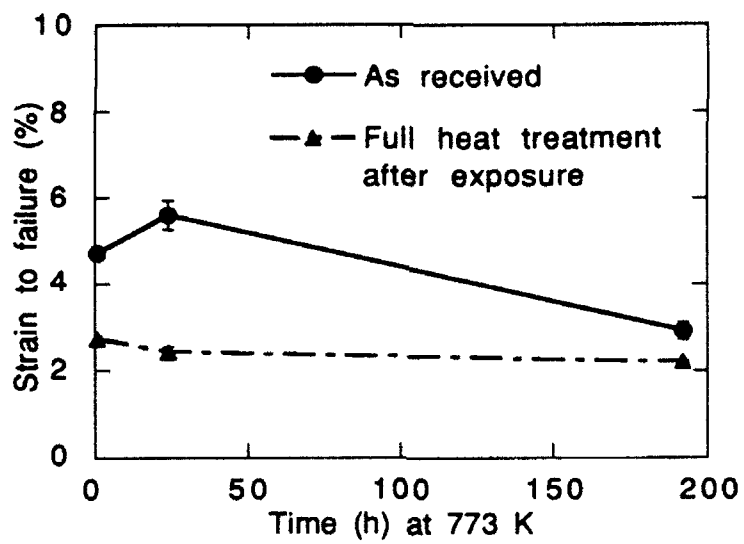
Fig. 12 Change in modulus versus number of thermal cycles from 298K to 77K.
Composites with reaction zone show large drop in modulus.



(a)

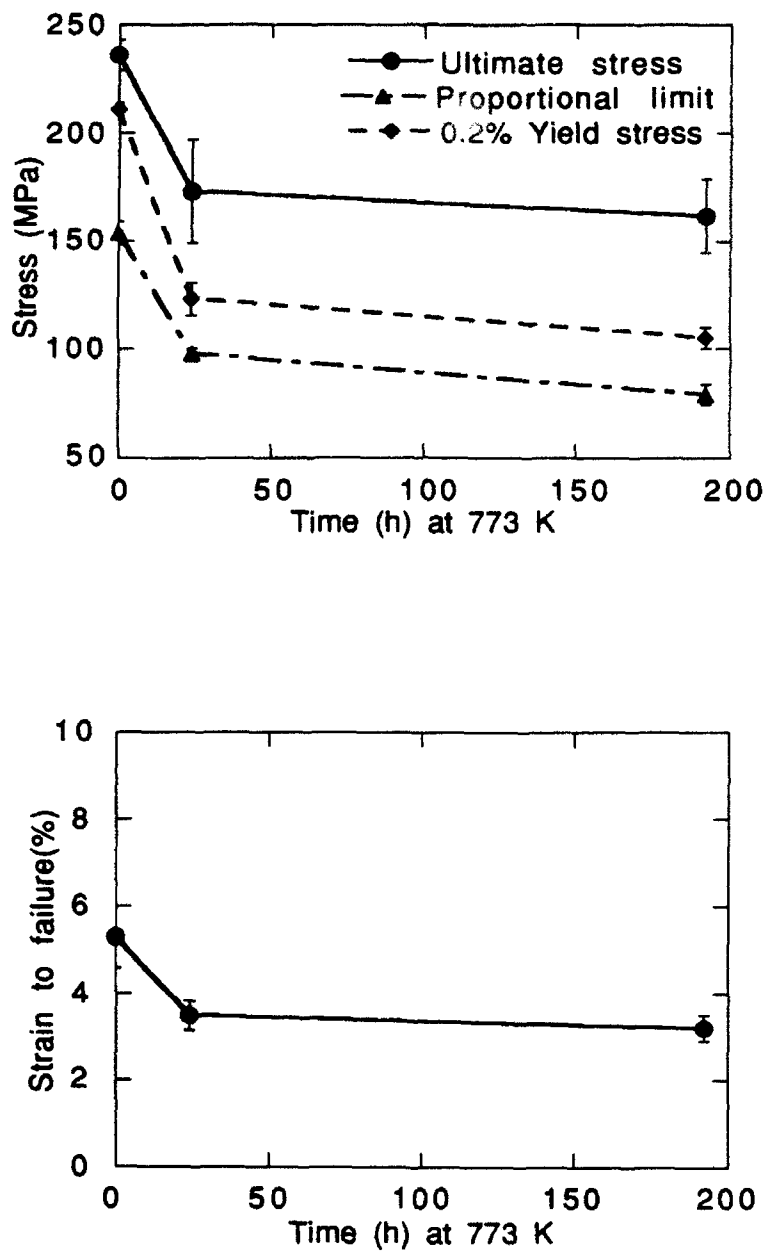


(b)



(c)

Fig. 13 Summary of Z6 / SiC tensile results. (a) Furnace cooled condition; (b) fully heat treated condition; (c) strain to failure versus time at 773K.



(b)

Fig 14 (a) Summary of EM31 / SiC tensile testing results versus time at 773K;
 (b) strain to failure.

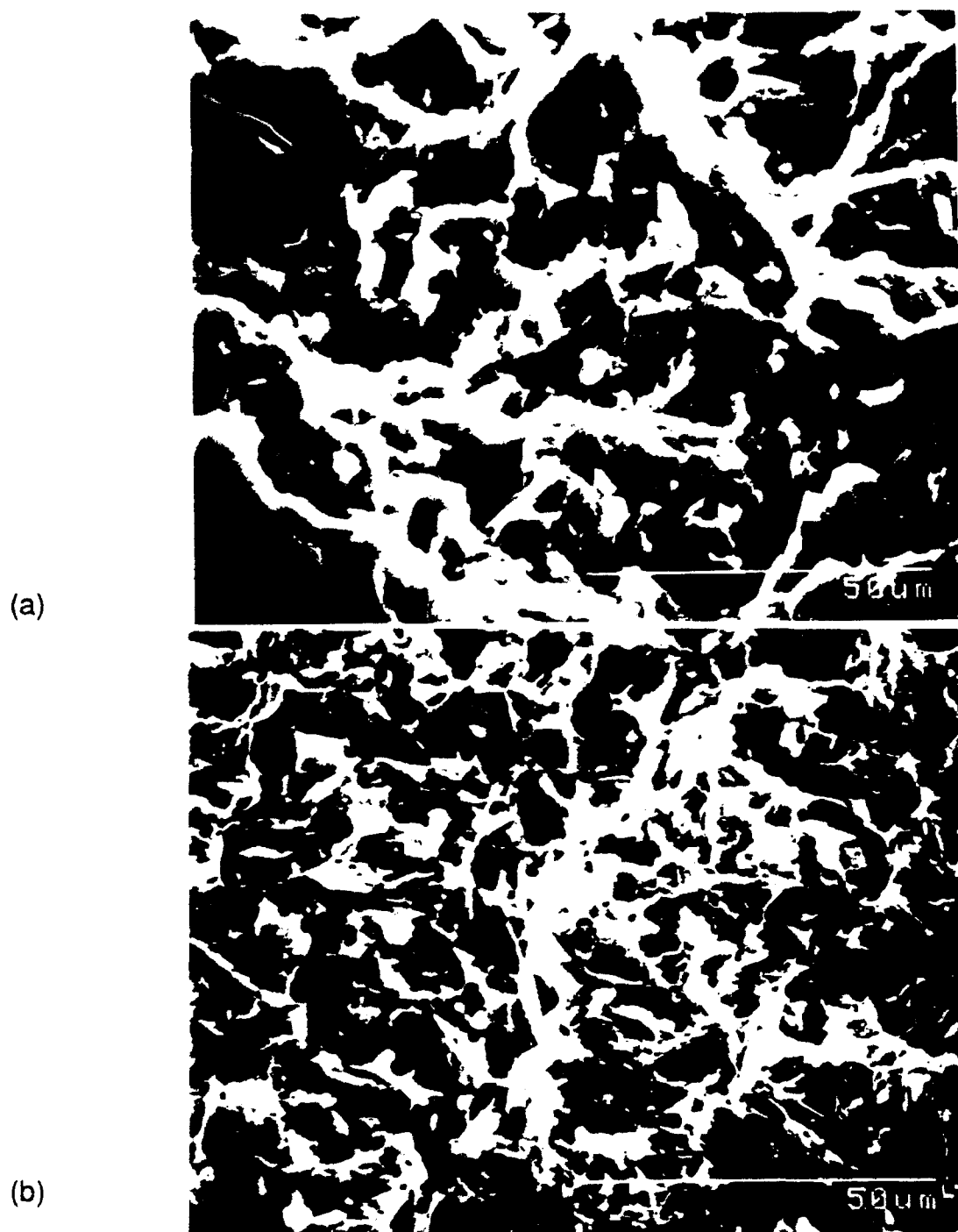


Fig. 15 SEM micrographs of Z6 / SiC fracture surfaces (a) 1 hour / 773K, (b) 192 hour / 773K. Note the increase in particle debonding and decrease in ductile tear ridges with increasing exposure.

III. MICROSTRUCTURE AND INTERFACES IN XD Al-TiC METAL MATRIX COMPOSITES

Rahul Mitra

TiC has a lower free energy of formation and is more stable thermodynamically than SiC, a more commonly used reinforcement in metal matrix composites. Thus it is possible to precipitate TiC particles by an exothermic *in-situ* reaction inside molten Al [1], but the same is not true for SiC. It is also a well known fact that TiC particles are sites for heterogeneous nucleation of Al grains during solidification [2] suggesting formation of low energy interfaces. Banerjee and Reif found that the effectiveness of TiC as a nucleant during solidification of Al is strong if the particles are precipitated *in-situ*, as this ensures TiC surfaces free of contaminants introduced by processing and oxides. Thus, Al-TiC metal matrix composites prepared by *in-situ* processes are of interest. However, the interfaces between Al and TiC have not been studied in the past, even though the interface plays a critical role in controlling the bulk mechanical properties of composites. Hence, this investigation aimed at characterization of Al/TiC interfaces as to structure, chemistry, mechanical behavior and thermodynamic stability.

Experimental Details

Extruded Al/TiC composites prepared by the XD process were obtained for this research from Martin Marietta Laboratory. High purity powders of C and Ti were mixed with Al (99.999% pure) and heated to a temperature above the melting temperature at which point the exothermic reaction ($Ti + C \rightarrow TiC$) takes place [1,3]. A master alloy was first prepared with a high volume fraction of TiC particles and then remelted with Al to obtain 0.15 volume fraction of dispersoid. The cast ingot was then extruded at 658 K to a ratio of 27:1. Average TiC particle diameter was either 0.7 μm with a standard deviation of $\pm 0.3 \mu m$ or $4 \pm 2 \mu m$.

The as-extruded composites were studied using conventional and high resolution transmission electron microscopy (CTEM and HRTEM). To obtain structural information from the interfaces using HRTEM, it is necessary to tilt the specimen such that both the metallic and ceramic phase are in low index zone axis orientation and the interface is parallel to the beam. As these conditions were not very frequently obtained in the present investigation, weak beam and ordinary dark field techniques were extensively applied to study the interfaces. Some as-extruded composite samples were pulled in tension to fracture or cold rolled and subsequently annealed to obtain recrystallization. Tension tests were carried out after annealing at 623 K for 30 minutes. Annealing was performed to relax residual stresses from extrusion and to obtain an equilibrium dislocation configuration. The microstructure and interfaces were observed and the results are summarized. Tension test was also performed at a temperature of 698 K.

Some of the samples of 0.7 or 4.0 μm particle sizes were heat treated at 913 K or 773 K from 24 to 496 hours and mechanical tests like hardness measurements, tension tests and modulus determination [4] were performed on these composites. The details of these experiments are cited in Ref. 5.

Results and Discussion

Microstructure and Interfaces

The sizes of the Al grains in the 0.7 μm particle size composite were 1.5-3.0 μm perpendicular to the extrusion direction and the particles were present both inside as well as at the Al grain boundaries as shown in Fig. 1. Figures 2(a) and (b) are SEM micrographs of 0.7 and 4.0 μm particle size composites respectively. Microstructure of the as-extruded Al-TiC has been reported in detail elsewhere [6]. The distribution of TiC particles was more or less uniform. As the reinforcements are precipitated *in-situ*, the surfaces of the particles do not have impurity phases on them and this results in direct contact on an atomic scale between the metallic matrix and the ceramic dispersoid. This

phenomenon is illustrated in Fig. 3, which shows a flat interface between Al and TiC in an XD Al-TiC composite with a particle size of 0.7 μm . While there is no obvious evidence of coherency across the interface (such as coherency strains or misfit dislocations), it is clear that there is intimate contact on an atomic level between the TiC particle and the Al matrix and TiC (111) plane is parallel to the interface. Most of the TiC particles observed have surfaces of {111} planes, which are close-packed and have either Ti or C atoms. From photoluminescence experiments [7], Ti-ended-TiC {111} surfaces are found to have electronic characteristics similar to Ti {0001} surfaces. Hence, it is believed that the TiC surfaces are comparable in activity to Ti, a situation that leads to metallic bonding between Al and TiC by electron transfer, provided the interfaces are clean. Bond strength or wetting characteristics can be further enhanced by the charged nature of defects in the ceramic reinforcement [8] near the interface as seen in the case of XD Al/TiC by the authors (Fig. 4) and also observed by Wang and Arsenault in XD NiAl/Al₂O₃ composite [9]. There is an increase in number of bonds at the interface, which may enhance the strength of the chemical bond.

Wolf [10] has shown that the asymmetric boundaries in metals and ceramics have a lower energy if one of the grains has a close-packed or low index plane parallel to the interface. Al-TiC interfaces are not symmetric because of differences in the interplanar spacings. The fact that the interface planes of TiC are densely packed thus assists in lowering the energy of the interface.

There are also boundaries with definite evidence of semicoherency as shown by the presence of misfit strain localization at the interface. Figure 5 shows that semicoherent boundaries can form between Al and TiC because of strong atomic interactions and tendency to lower the interfacial energy.

The as-extruded 15 vol% XD Al-TiC composite has shown excellent ductility and can be cold rolled without interfacial cracking to 75% reduction. Figure 6 shows the microstructure after cold rolling where subgrains can be seen around the particles.

These form by dynamic recovery in the matrix around the particles leading to low energy dislocation configurations. Subsequent annealing at 773 K leads to recrystallization with further formation of Al subgrains around TiC particles. Many of the particles and subgrains have semicoherent interfaces between them as shown in Fig. 7 by the strain contrast observed at the interfaces. Similar structures were seen at many other interfaces between TiC particles and Al subgrains. The average spacing between the dislocations varies between 10 and 50 nm suggesting different degrees of coherency. Also the strain contrast is not fully periodic. But the localized nature of strain contrast at the interface proves that the planar misfit is accommodated by localized distortions in the lattice of Al and the interface is semicoherent. These dislocations can not be caused by differences in thermal expansion coefficient of Al and TiC (1:4) as such dislocations are lattice dislocations and randomly arranged.

From a large number of observations, it can be inferred that during recrystallization of the cold deformed Al-TiC, there is a tendency for Al subgrains to nucleate at the TiC particles forming semicoherent interfaces. *In-situ* processing allows atomistic interaction between Al and TiC as a result of which the interface tends to reach an equilibrium condition and relaxation of atomic positions next to the interfaces takes place to lower the interfacial energy. Few interfaces showed any cracking after 75% reduction, except those at clusters proving that the strain energy necessary for particle-matrix debonding is very high. Good bonding across the interface, which has a high metallic character, is thought to be responsible for the high toughness of the interfaces and formability of the composite.

Mechanical Characterization

Room temperature tension test results are shown in Table I. For the purpose of comparison, the mechanical properties of commercial Al are also shown in Tab. I. Both the composites have shown remarkable elongation properties, inspite of the fact that volume fraction of the particles is 15%. A TEM investigation of the deformed regions of the composite showed high dislocation density resulting in deformation zones around particles. No voids were seen at a region with reduction in area of 15%. Figure 8 shows a representative micrograph of the strained material. At higher strains (20% reduction in area), the matrix cracks by a tearing mechanism as shown in Fig. 9. The interface between the Al and TiC thus has the ability to withstand extensive shear allowing local lattice rotation in the matrix without fracture. In contrast to this, *in-situ* tension studies by Ruedl [11] for Al with 2.5 vol.% of submicron Al_2O_3 particles in the TEM showed a large amount of interfacial cracking. The interface was not resistant to fracture. Similar particle-matrix debonding has been seen in the interfaces of Cu- SiO_2 [12] and Al alloys containing inclusions [13]. The particles in these investigations were also of submicron size. Thus, the interface structure and nature of bonding plays a significant role in determining the energy needed for decohesion between particle and matrix.

Annealing of the room temperature tension tested sample leads to the evolution of a microstructure similar to that obtained on annealing after cold rolling. The particles are surrounded by subgrains. Presence of fresh grains proves that recrystallization takes place. Figure 10 shows a representative TEM micrograph of the microstructure. At high temperatures, elongation achieved is very large because of dynamic recrystallization in the matrix around the particles. The ability of the matrix to recrystallize and high toughness of the interface is responsible for high ductility with a significant improvement in strength over that of pure Al.

The Young's modulus value of the composite was found to be 93.8 GPa [6], which is within the lower and upper bounds expected for 15 vol% Al-TiC from Hashin

and Shtrikman's relations [14]. This proves that the bond integrity at the interface is excellent. In general, XD composites have shown higher Young's modulus values than those prepared by conventional mechanical mixing processes [15].

The interfacial energy was calculated for a number of particles by measuring the contact angles between the interfacial voids (generated during cold rolling at clusters or during high temperature tension tests at grain boundaries) and the TiC particles. A contact angle is defined as the angle between the tangent to the void surface and the facet of the particle as shown in Fig. 11. The interfacial energy is given by:

$$\gamma_{pm} = \gamma_{pv} + \gamma_{mv} \cos \theta \quad \dots\dots(1)$$

where γ_{pm} is the particle-matrix interfacial energy, γ_{pv} and γ_{mv} are the surface free energies of the particle and the matrix, respectively. The energies measured in as-extruded 0.7 μm particle size composite varied between 200 and 800 mJm^{-2} possibly depending on the interface structure (different degrees of coherency) and nature of chemical bonding (electronic structure of the interface). Most particles did not show any decohesion.

Chemical Reaction Strengthening

Figures 12(a) and (b) shows the microstructure of the composite after heat treating for 96 and 336 hours at 913 K, respectively whereas Fig. 13 shows a backscattered SEM image of the 4.0 μm particle size composite after heat treating for 264 hours at 913 K. Significant increase in the volume fraction of the reaction products took place with increase in the time of heat treatment in the 0.7 μm particle size composites, while this was confined only to the interfaces in the 4.0 μm particle size composites.

This happened at 913 K because Al and TiC do not coexist in thermodynamic equilibrium at all temperatures, even though TiC has a free energy of formation much lower than that of Al_4C_3 [16]. At temperatures below 1025 K, the reaction:



has a negative free energy change. This is shown in Fig. 14(a). Reactions (2) and (3) in Fig. 14(a) which lead to formation of other kinds of reaction products have positive free energy change. Figure 14(b) shows a ternary Al-Ti-C phase diagram for 913 K. The equilibrium atomic concentration of Al, Ti and C lies in triangle I of Fig. 14(b), as a result of which Al_3Ti , Al_4C_3 and Al are the equilibrium phases. Thus, during heat treatment at 913 K, TiC and Al reacted to form Al_3Ti and Al_4C_3 . Some Ti_2AlC and TiAl particles could also be seen possibly due to inhomogeneities in composition created by clustering of TiC particles. This leads to a situation where the local atom fraction of the components lies in other triangles. Figs. 15(a-d) are TEM micrographs of Al_3Ti , Al_4C_3 , TiAl and Ti_2AlC particles, respectively. The phases have been identified using selected area electron diffraction. X-ray diffraction was also performed on all samples. 4.0 μm particle size composite showed only Al_3Ti and Al_4C_3 other than Al and TiC.

The changes in the microstructure are interesting as these resulted in a remarkable increase in the Young's modulus and room temperature tensile strength and microhardness of the composites with increase in time of heat treatment. Similar trends in properties were seen also at higher temperatures. Figures 16-19 show the variation of Young's modulus, room temperature hardness, room temperature tensile strength and high temperature hardness with heat treatment of the 0.7 or 4.0 μm particle size composites, respectively. This was, however, at the cost of room temperature ductility as the reaction products were brittle and randomly oriented as is clear from room temperature engineering stress-strain curves of Fig. 20. Fracture takes place by breaking of the intermetallics. At higher temperatures, ductility improved in the heat treated composite as shown in Fig. 21. The tensile strength of the 96 hours heat treated 0.7 μm particle size composite is significantly larger than that of cast and extruded composite. This suggests that the as-extruded 0.7 μm particle size composite which is ductile at room temperature and even more formable at higher temperatures can be

formed into any shape and heat treated for an appropriate length of time to achieve high strength and modulus for practical use. For room temperature use, 24 hours of heat treatment appears to be appropriate to optimize strength and ductility as is clear from room temperature stress-strain curves of Fig. 20.

REFERENCES

1. A. R. C. Westwood, Metall. Trans. 19A: 749-758 (1988).
2. A. Banerji and W. Reif, Metall. Trans. 17A: 2127-37 (1986).
3. R. M. Aikin, Jr., Martin Marietta Laboratory, Baltimore, MD. Private Comm.
4. M. E. Fine, ASTM STP, 129: 1-43 (1952).
5. R. Mitra, J. R. Weertman, M. E. Fine and R. M. Aikin, Jr., in Developments in Ceramic and Metal-Matrix Composites, edited by K. Upadhyaya (TMS, Warrendale, PA, 1992) 125-142.
6. R. Mitra, W. A. Chiou, M. E. Fine and J. R. Weertman, submitted to J. Mater. Res.
7. A. M. Bradshaw, J. F. Van der Veen, F. J. Himpel and D. E. Eastman, Sol. State Comm., 37: 37-40 (1980).
8. A. M. Stoneham and P. W. Tasker, J. Phys. C18: L543-L547 (1985).
9. L. Wang and R. J. Arsenault, Metall. Trans. 22A: 3013-18 (1991).
10. D. Wolf, in Ceramic Microstructures '86: Role of Interfaces. Materials Science Research 21, edited by J. A. Pask and A. G. Evans (Plenum Press, New York, 1986) 177-185.
11. E. Ruedl, J. Mater. Sci. 4: 814-816 (1969).
12. F. J. Humphreys and A. T. Stewart, Surf. Sci. 31: 389-421 (1972).
13. D. Broek, Engng. Fract. Mech. 5: 55-66 (1973).
14. Z. Hashin and S. Shtrikman, J. Mech. Phys. Sol. 11: 127-140 (1963).
15. A. R. C. Westwood and S. R. Winzer, in Advancing Materials Research, edited by P. A. Paras and H. D. Langford (Nat. Acad. Press., Washington, D. C., 1987) 225.

16. I. Barin, Thermochemical data of pure substances, Weinheim, Germany: VCH Verlagsgesellschaft, 17, 26, 71, 72, 1520, 1528 (1989).

TABLE I. Stress strain data of commercially pure Al and XD Al/TiC composite.

Specimen Type	YS (MPa)	UTS (MPa)	Elong. (%)	Strain Hardening Expon. (n)
1050-Al(O)	28.0 ⁸	76.0 ⁸	39.0 ⁸	
1100-Al(O)	35.0 ⁸	90.0 ⁸	45.0 ⁸	0.24 ⁹
Al-15 vol.% TiC				
0.7 μm size	110.0	154.5	20.0	0.19
(as-extruded and annealed at 623 K for 0.5 h and tested at 298 K)				
Al-15 vol% TiC				
4.0 μm size	66.0	131.5	23.1	0.18
(as-extruded and annealed at 623 K for 0.5 h and tested at 298 K)				
Al-15 vol.% TiC				
0.7 μm size	21.0	32.1	56.0	not applicable
(as-extruded and tested at 698 K; total time at 698 K was about 20 min.)				



Fig. 1. TEM micrograph of an Al grain with TiC particles. The particles lie both inside as well at grain boundaries.

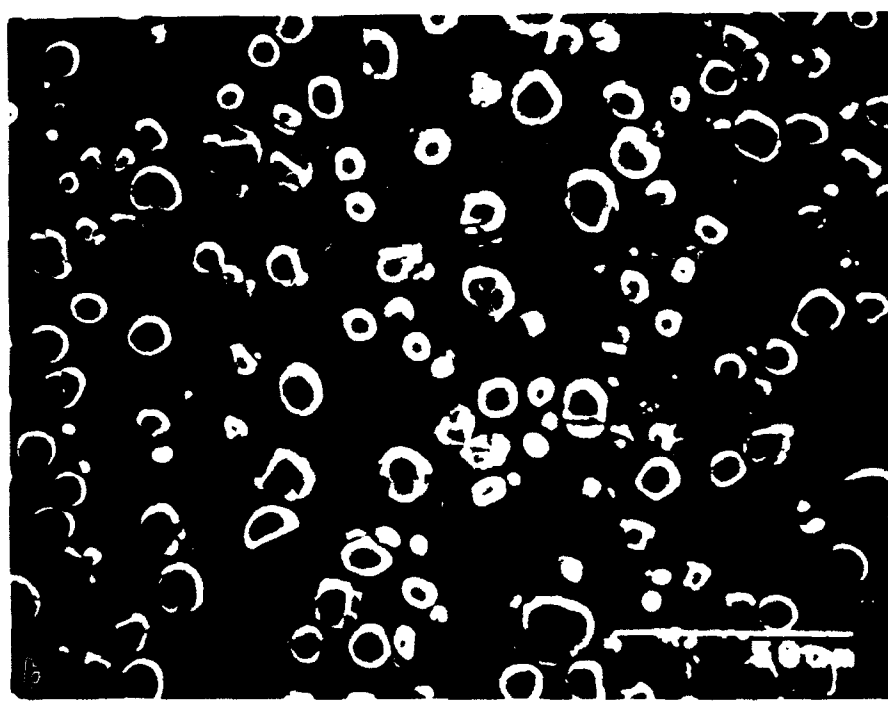
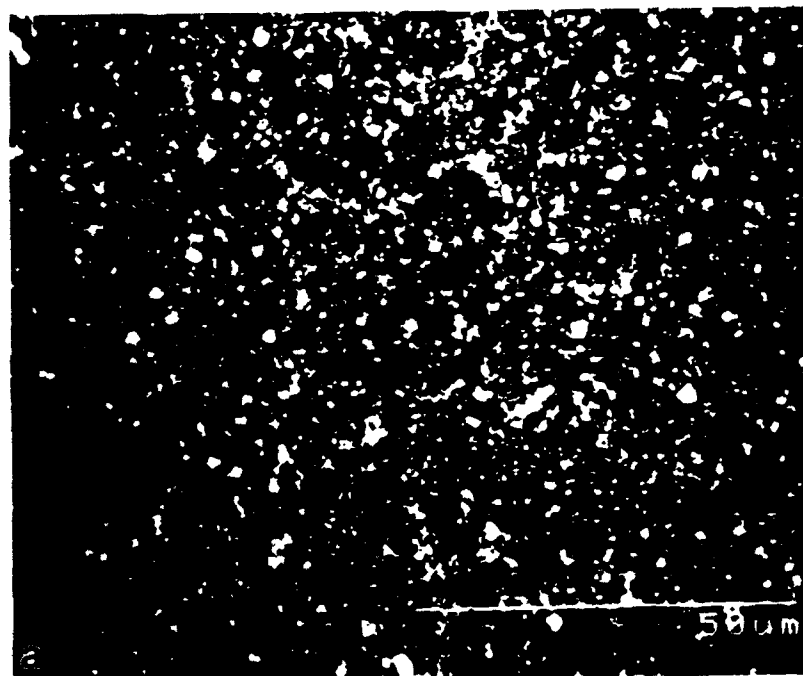


Fig. 2. SEM micrographs of the as-extruded XD Al/TiC metal matrix composites: (a) 0.7 μm particle size and (b) 4.0 μm particle size. The distribution is uniform.

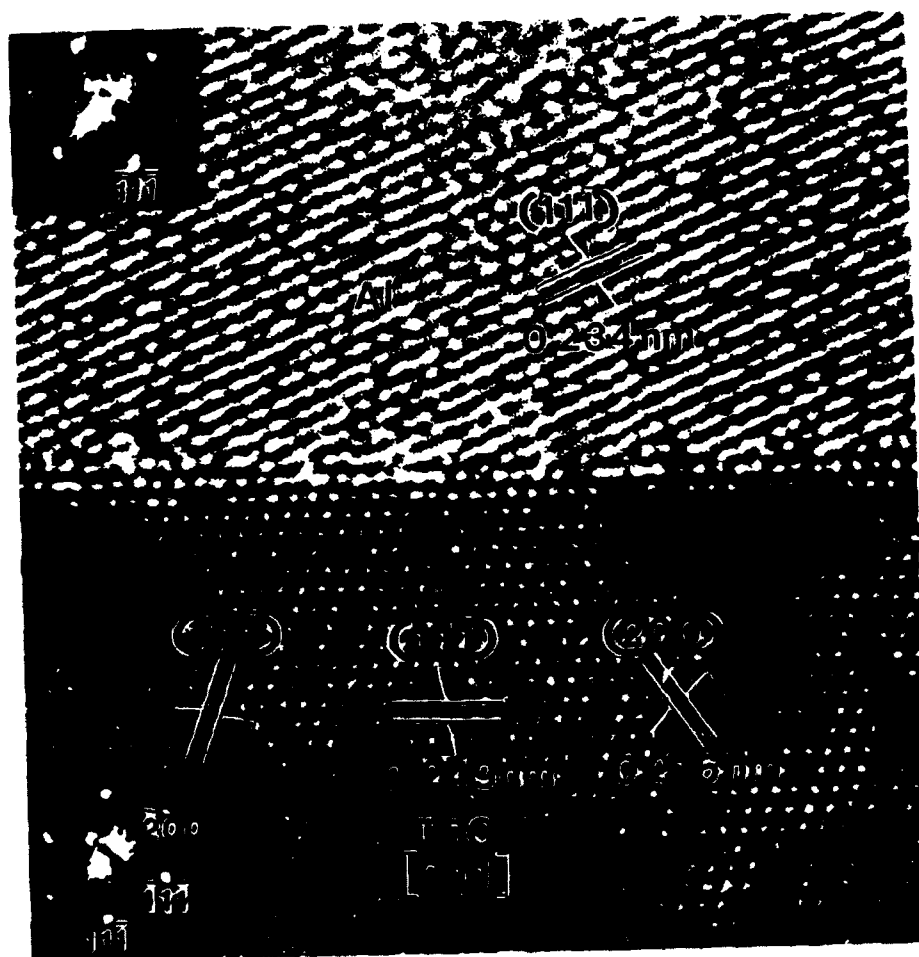


Fig. 3. High resolution TEM micrograph of a flat interface in the as-extruded 0.7 μm particle size composite. The interface is atomically abrupt with direct contact between Al and TiC.

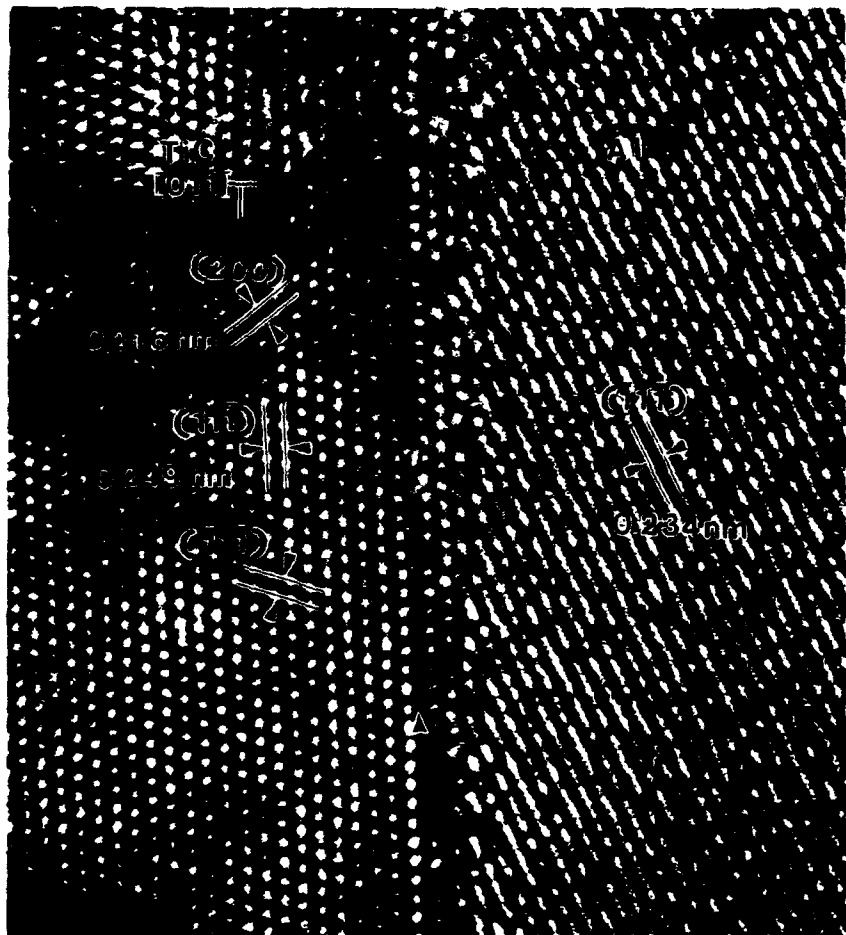


Fig. 4. High resolution TEM micrograph of an interface in the as-extruded 0.7 μm particle size composite. The first three layers of atoms inside the TiC near the interface are distorted because of the presence of a stacking fault on the $(\bar{1}\bar{1}\bar{1})$ planes. An edge dislocation can also be seen.

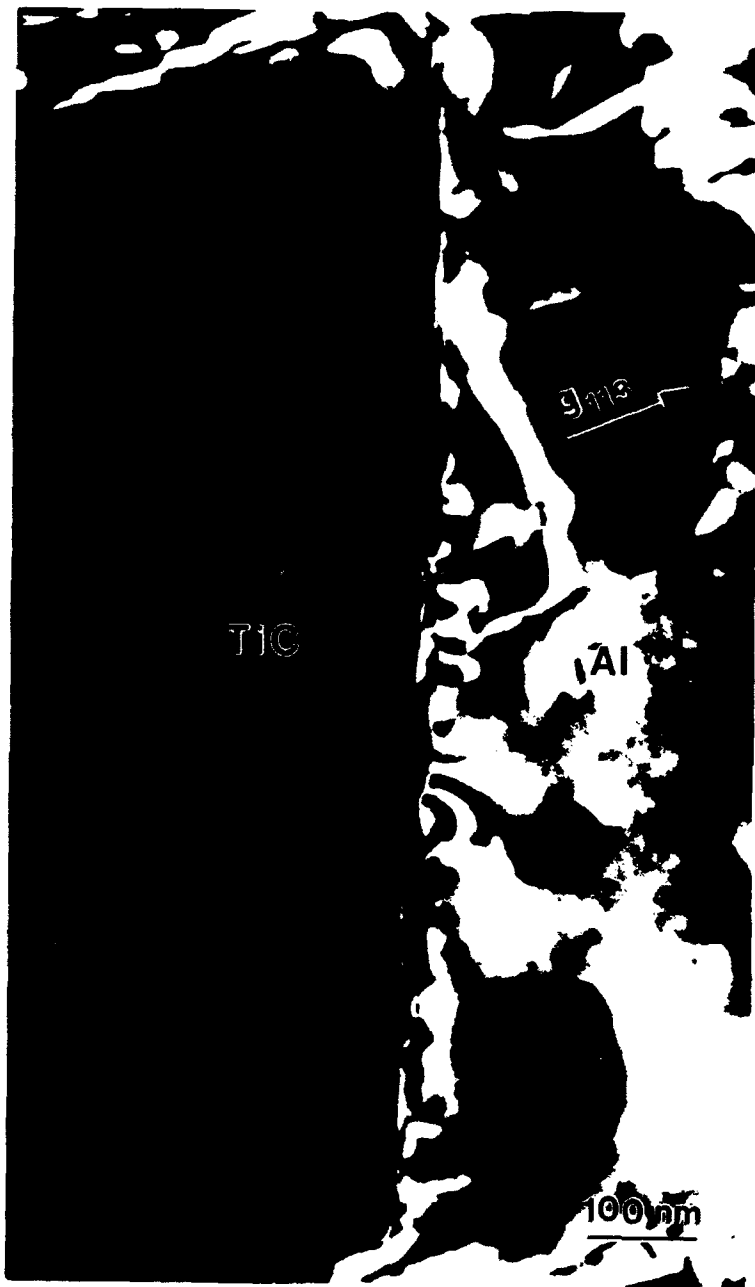


Fig. 5. Weak beam dark field TEM micrographs of semicoherent interfaces in the as-extruded Al/TiC composite. Misfit strain localization can be seen.



Fig. 6. Subgrains formed around TiC particles by dynamic recrystallization during cold rolling to 75% reduction. Interfacial cracks could not be seen other than at clusters.



Fig. 7. Interface between an Al subgrain formed at Al/TiC interface after 75% cold rolling and annealing. The presence of misfit strain localization proves that the interface is semicoherent.



Fig. 8. TEM micrograph with 15% reduction in area. There is high dislocation density surrounding the particles forming deformation zones.



Fig. 9. TEM micrograph from a region with 20% reduction in area. The region around the particles undergo extensive shear and become misoriented with respect to neighboring area. Crack propagates in the Al matrix by a ductile tearing mechanism.



Fig. 10. TEM micrograph of a tension tested sample, which was annealed subsequently at 773 K for 1 hr. Fresh grains appear and are broken up into subgrains.

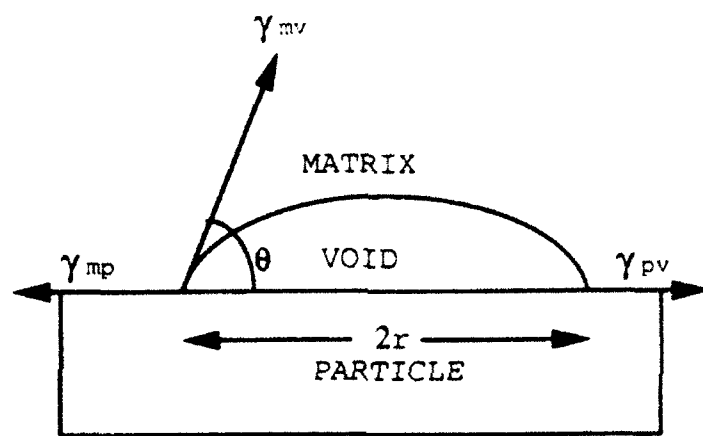


Fig. 11. Schematic diagram of a void formed at the interface between the facet of a particle and the matrix.

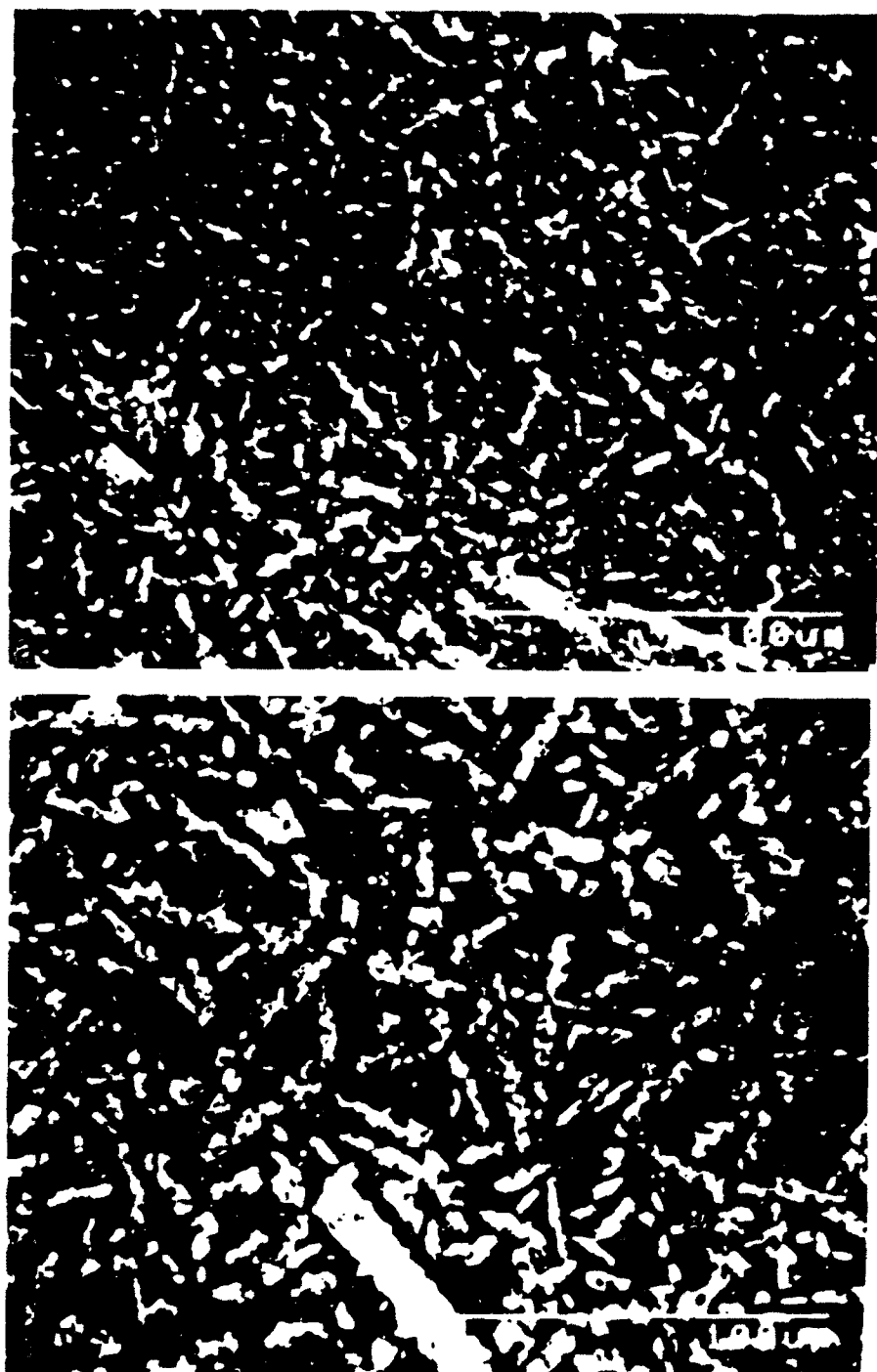


Fig. 12. SEM micrograph of the $0.7 \mu\text{m}$ particle size XD Al/TiC composite heat treated at 913 K for (a) 96 hours and (b) 336 hours. The high aspect ratio particles are intermetallics growing from chemical reaction between Al and TiC.

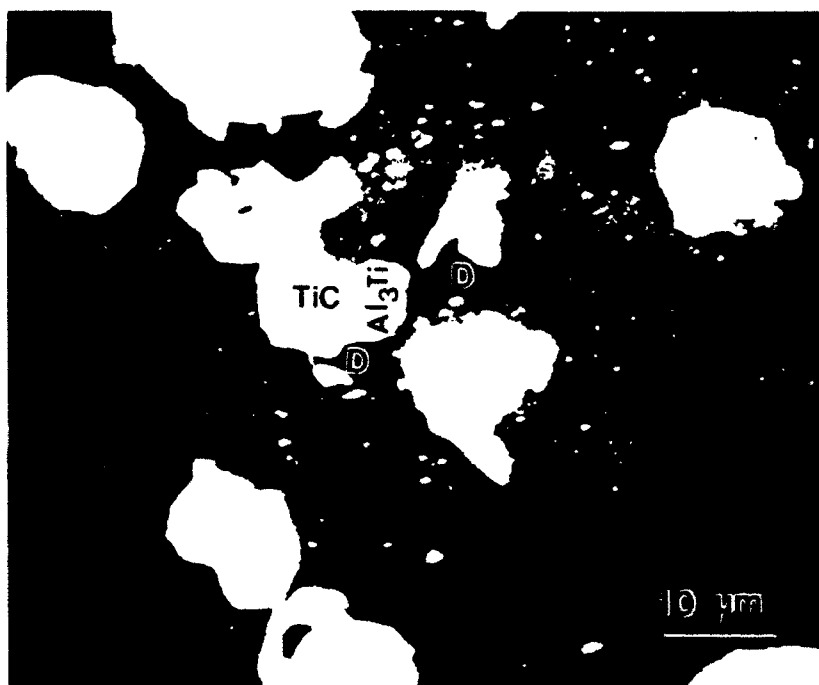
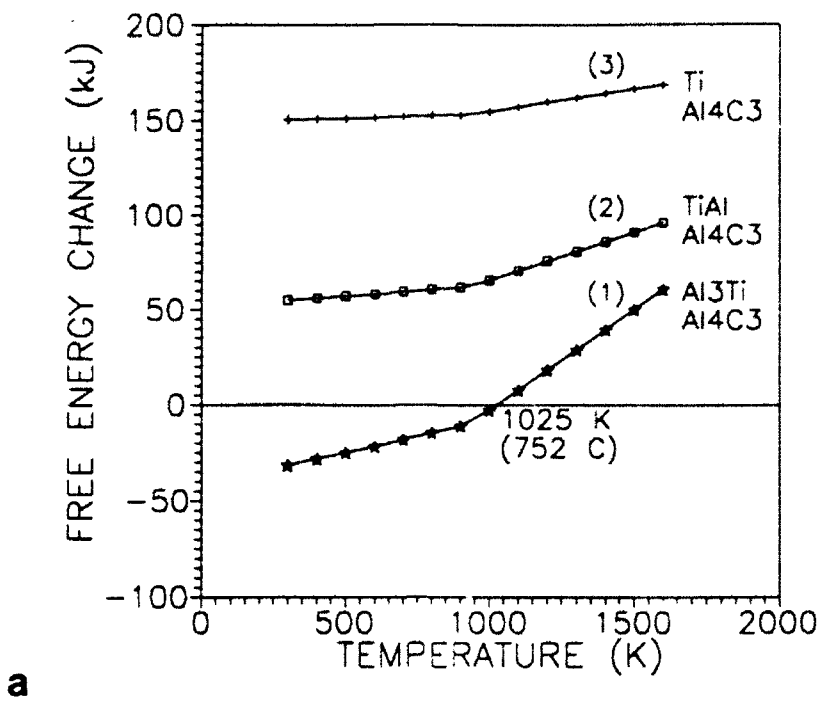


Fig. 13. Backscattered SEM image of the 4.0 μm particle size composite showing reaction products at the interface. EDAX (with Be window) analysis has shown that the lighter area next to TiC particles contains Al and Ti, whereas TiC has only Ti. From X-ray diffraction results, it is concluded that these must be Al₃Ti as other Al-Ti compounds are absent. The area marked 'D' is darker than Al and is thought to be Al₄C₃.



a

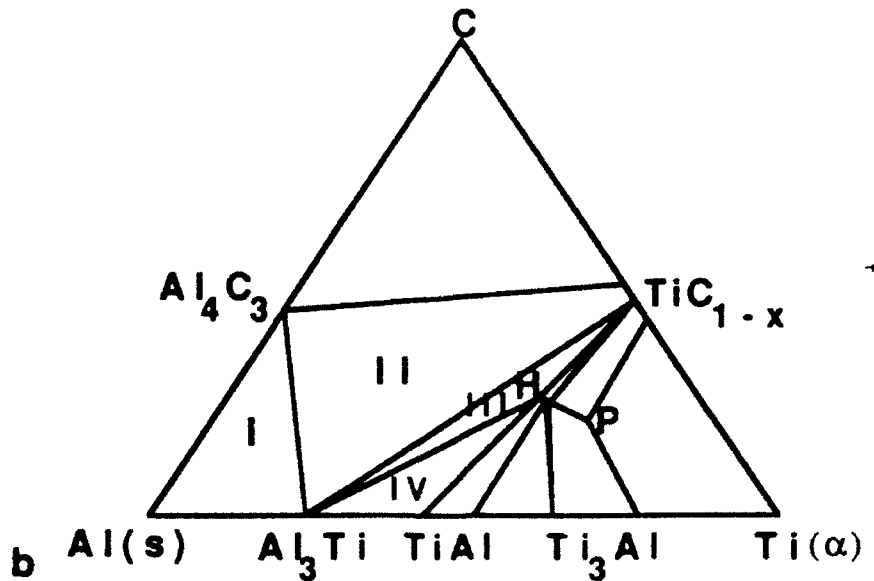
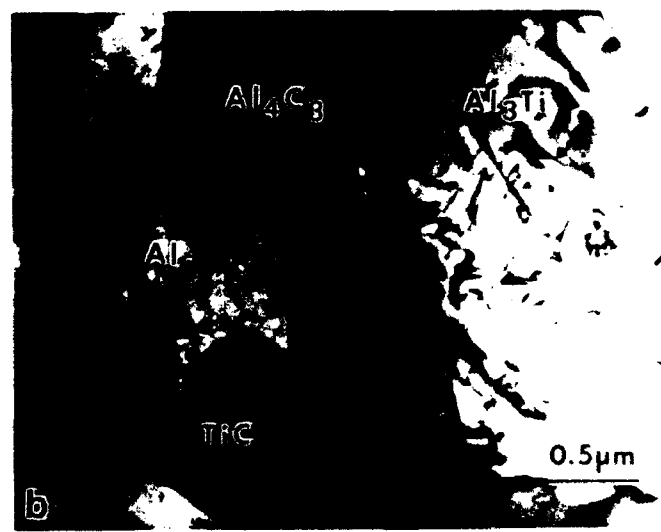
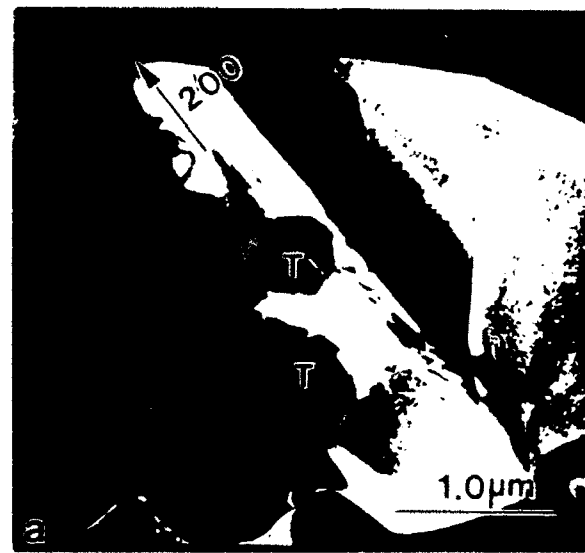


Fig. 14. Thermodynamic analysis: (a) Free energy versus temperature diagram for 3 different reactions between Al and TiC with products: (1) Al_3Ti and Al_4C_3 ; (2) Al_4C_3 and Ti and (3) Al_4C_3 and TiAl . (b) Ternary phase diagram of Al-Ti-C system for 913 K.



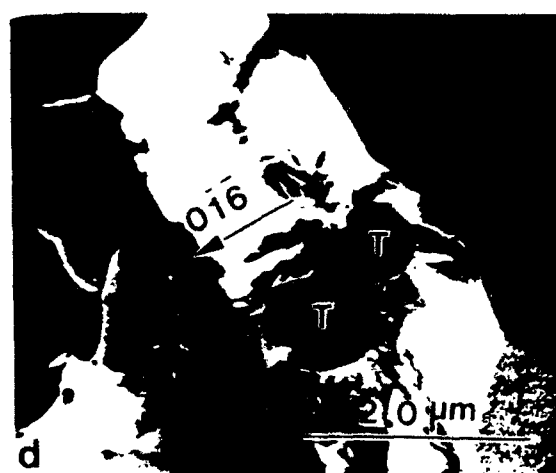


Fig. 15. TEM micrographs of reaction products: (a) Al_3Ti , (b) Al_4C_3 , (c) TiAl and (d) Ti_2AlC .

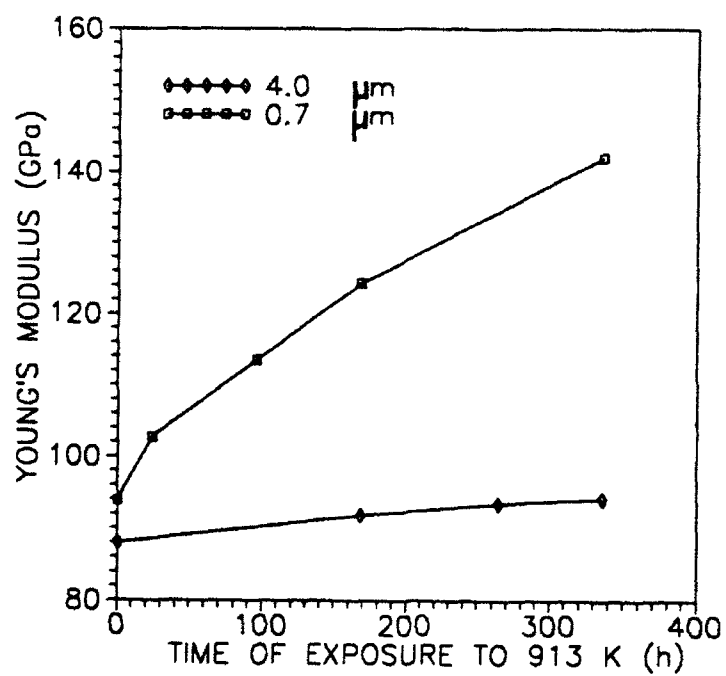


Fig. 16. Variation of room temperature Young's modulus of 0.7 μm and 4.0 μm particle size composite with increase in time of heat treatment at 773 K and 913 K.

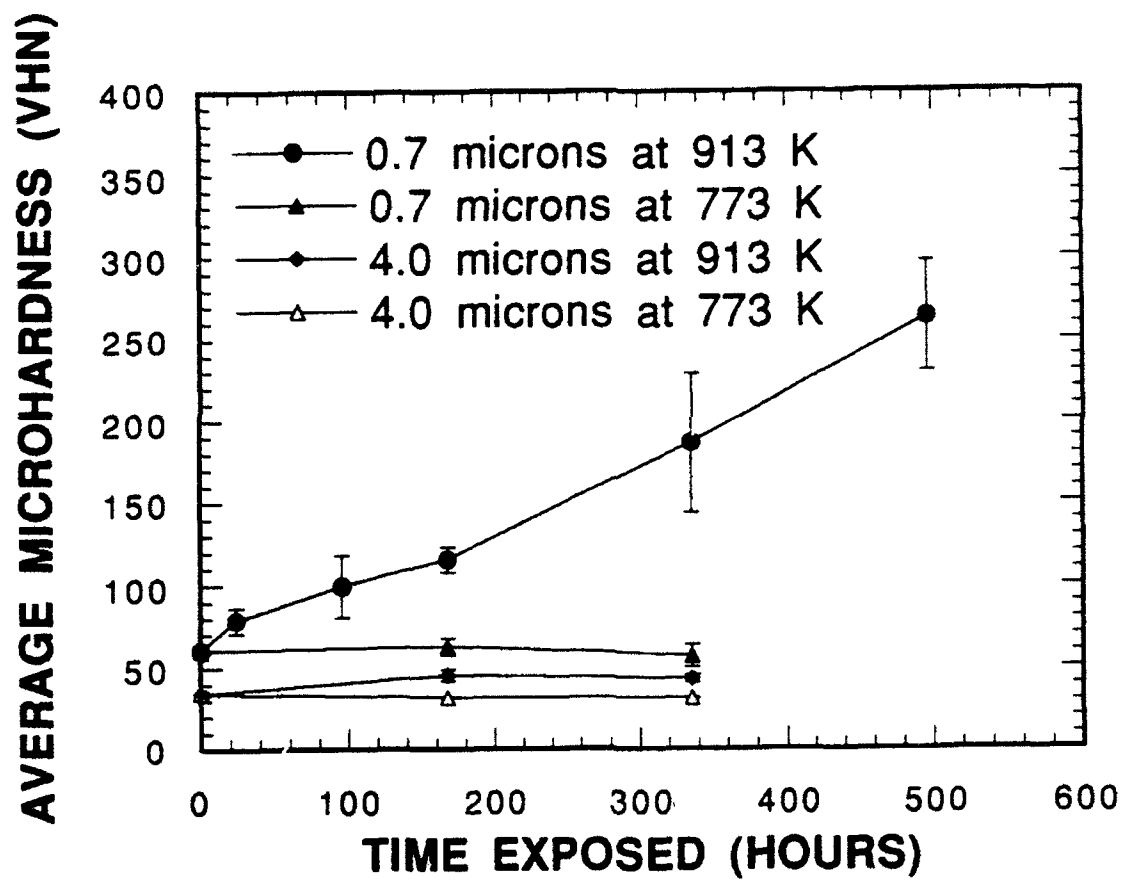


Fig. 17. Variation of room temperature microhardness with increase in time of heat treatment at 773 K and 913 K.

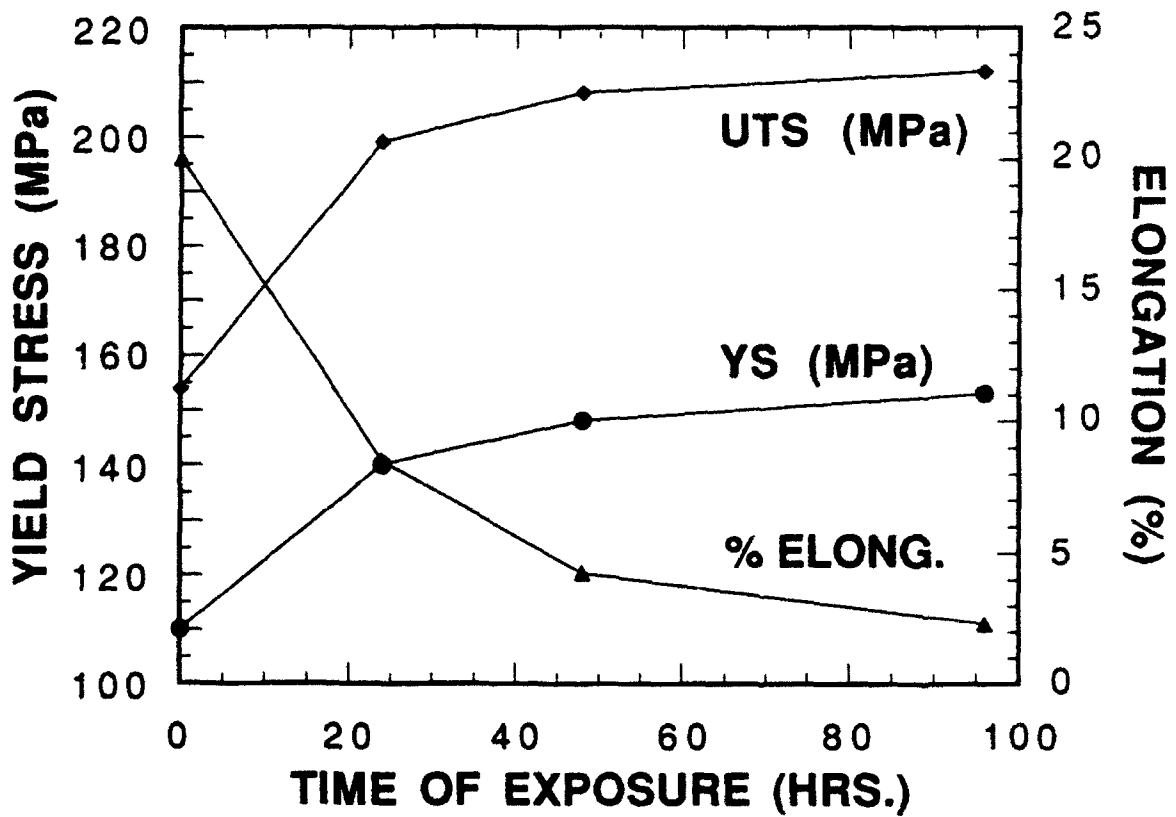


Fig. 18. Variation of room temperature tensile strength and percentage elongation with an increase in time of heat treatment at 913 K.

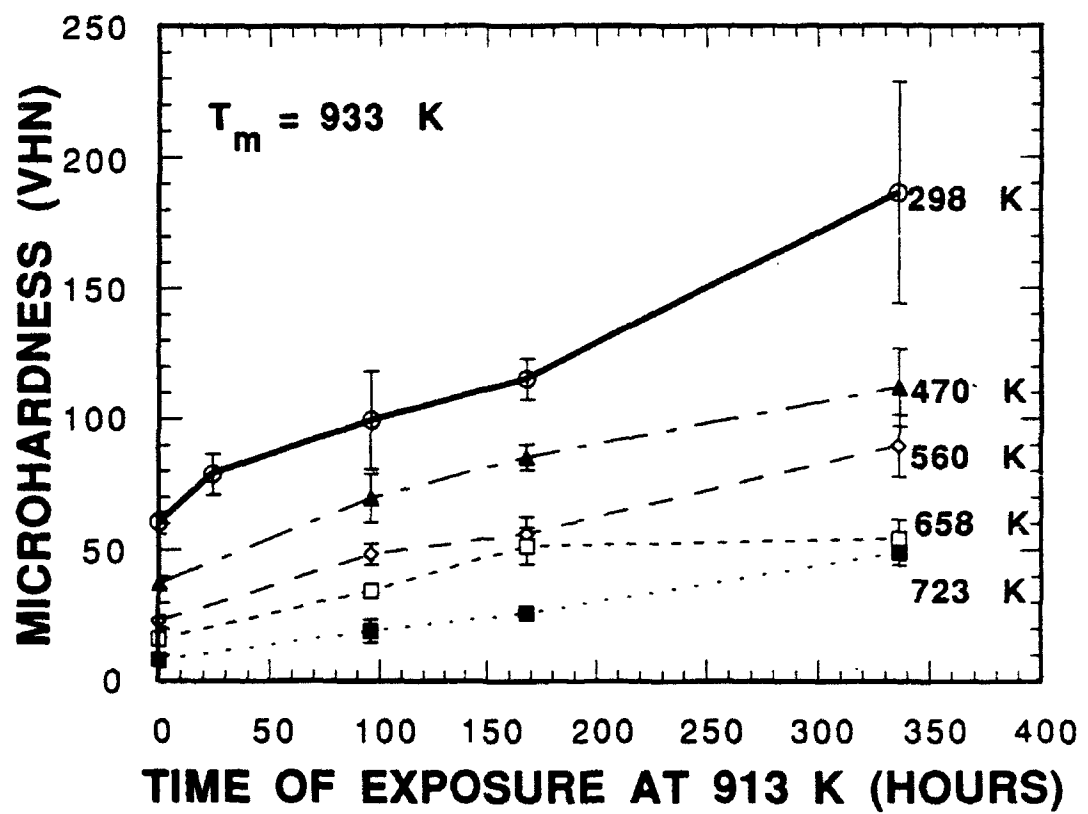


Fig. 19. Variation of high temperature hardness with an increase in time of heat treatment at 913 K.

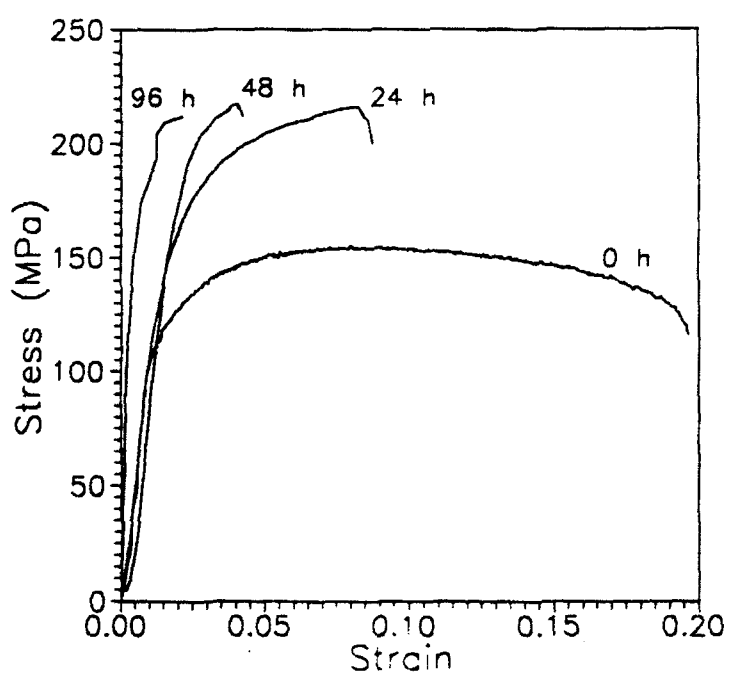


Fig. 20. Room temperature engineering stress-strain curves for samples heat treated from 0 to 96 hours at 913 K.

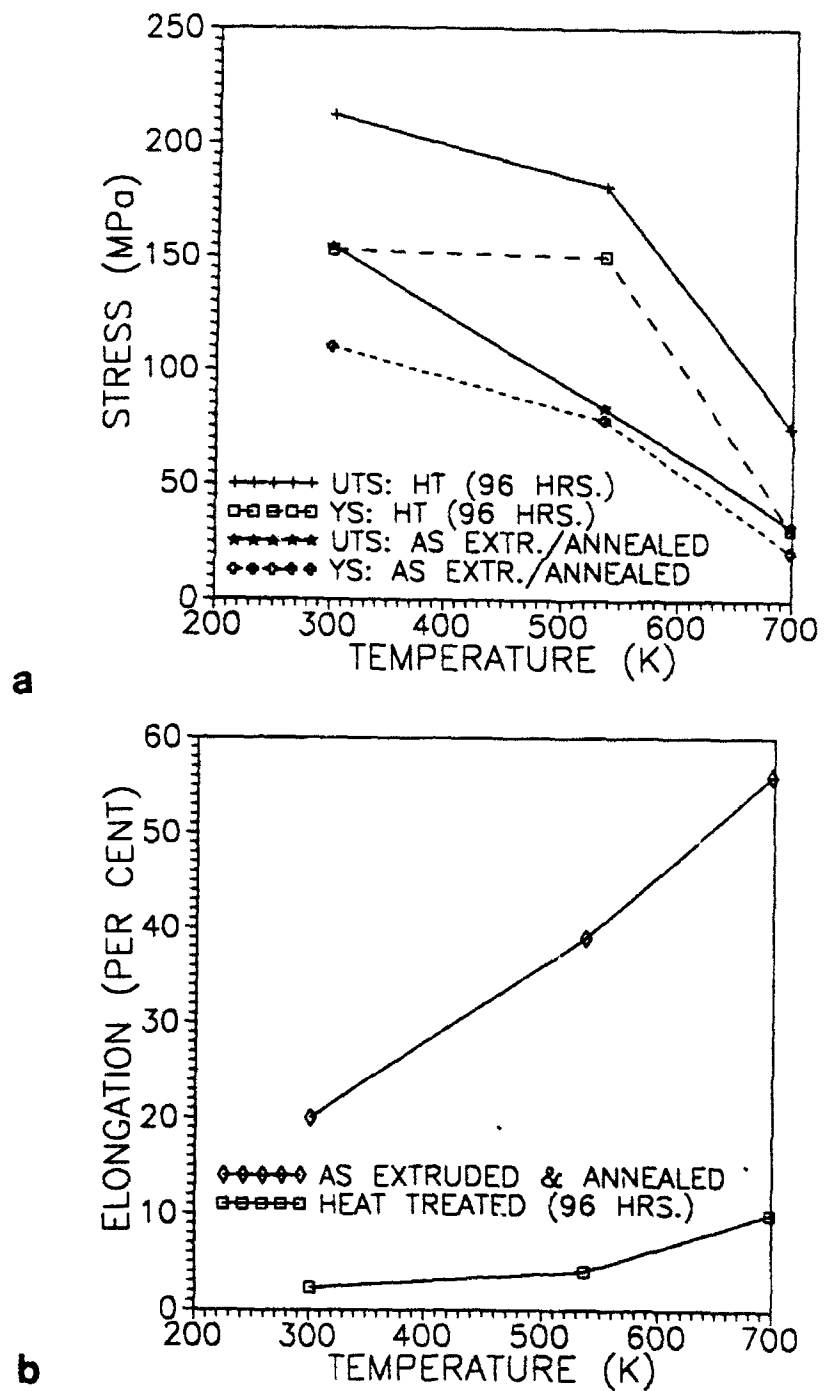


Fig. 21. High temperature tension test: (a) Variation of yield and ultimate tensile strengths and (b) percentage elongation with absolute temperature of the 0.7 μm particle size composite after heat treatment at 913 K for 0 and 96 hours.

IV. DUCTILITY OF CAST Al-Al₃Zr_xTi_{1-x} COMPOSITES, P. A. Earvolino

1. Introduction

Metal-matrix composites (MMC's) may offer improvements in strength, modulus, and creep resistance compared to the properties of the unreinforced matrix material. A problem common to most MMC's, however, is their poor ductility, which is attributed to the brittleness of the dispersed phase and the brittleness or weakness of the particle/matrix interface. MMC's are most frequently prepared by powder metallurgy techniques and the resulting material is expensive. In a sense many two-phase metallic alloys such as steels are composites, with the second phase separating from the liquid during solidification or from the solid by precipitation. Such alloys generally have better interfacial properties than conventional MMC's and their microstructures may be refined by thermomechanical processing with less or no interface cracking.

A composite consisting of Al₃Zr_xTi_{1-x} crystallites in an Al matrix may be made by conventional casting and rolling even though the intermetallic is itself brittle. The structure of the Al₃Zr_{0.25}Ti_{0.75} intermetallic is that of Al₃Zr, i.e., tetragonal DO₂₂ with Ti atoms replacing Zr atoms in the lattice.

The selection of Al₃Zr_xTi_{1-x} for this study was based on previous research. The lattice parameters of the DO₂₂ structured Al₃Ti, a' and c, are comparable to a₀ and 2a₀ (where a₀ is the lattice parameter of cubic Al and a' is the half diagonal length of the (001) plane in the Al₃Ti unit cell): a' is 5% less than a₀, and c is 6% more than 2a₀. In Al₃Zr (DO₂₂), isostructural to Al₃Ti except for a modulation along the c axis, a (not a') is 1% less than a₀ of aluminum, but c is 7% greater than 4a₀ (1). By alloying with Ti the overall mismatch was reduced; Tsunekawa and Fine (2) determined that in the Al₃Zr_xTi_{1-x} intermetallic compound, decreases in x only slightly increased the mismatch between a of Al₃Zr_xTi_{1-x} and a₀ of aluminum, while the mismatch in the c parameter (as compared to 4a₀) was reduced considerably. At x = 0.25, the mismatch in c is 4%, in a is 3%. Presumably, improvements in lattice matching should result in better interfacial properties; however, a study to test this hypothesis has not been completed.

2. Experiment

Samples of the Al/Al₃Zr_{0.25}Ti_{0.75} and Al/Al₃Zr_{0.75}Ti_{0.25} metal-matrix composites have been prepared by nonconsumable tungsten arc-melting under a purified argon atmosphere, with a water-cooled copper crucible used as the cathode. Initial components are chips of 99.999% Al, granules of 99.9% Ti, and shavings of 99.9% Zr. The melted buttons are flipped and melted ten times to insure compositional homogeneity.

Two Al/Al₃Zr_{0.25}Ti_{0.75} (15v/o) samples, each weighing 8g and having a thickness of 10.1 mm, were annealed at 500 °C for one hour and then hot-pressed at 500 °C to a final reduction in thickness of 59%. One sample was sectioned, mounted, and polished for optical microscopy (sample I); as with all of the other samples prepared for microscopic investigation, sample I was not annealed immediately prior to sectioning. The other sample was exposed to a regimen of cold-rolling and intermittent annealing. After an initial one hour anneal at 400 °C, the sample was passed through a rolling mill. With each pass, the thickness of the sample was reduced by approximately 64 µm (2.5 mils). After five passes, the sample was exposed to a 10 minute anneal at 400 °C. This procedure was repeated until the thickness of the sample was 0.50 mm, a reduction in thickness of 95%. A portion of this sample was then sectioned and prepared for optical microscopy (sample II). The remainder of the sample was then cold-rolled (small diameter working rolls were used to enable the further deformation of the increasingly thin material) to a final thickness of 26 µm, representing a total reduction in thickness of 99.74%. No annealing was necessary. Again, a portion of the sample was taken for microscopic observation (sample III). Subsequent deformation of the sample was achieved by folding and rolling it, again without annealing. The two folded halves are thus stuck together after rolling. In this manner, the effective thickness of the sample is reduced by a factor of

two after each pass. A total of four passes was made, thereby resulting in a sample 1/16th as thick as the starting 26 μm foil. This amounts to an effective thickness of 1.6 μm , representing a total reduction of 99.983%, i.e. the thickness was only 0.017% of the original thickness.

A third Al/Al₃Zr_{0.25}Ti_{0.75} (15v/o) sample, weighing 8g and having a thickness of 10.1 mm, was hot-pressed, as above, to a total reduction in thickness of 59% and then cold-rolled to a thickness of 0.50 mm, a total reduction in thickness of 95%. The sample was then wire-cut into "dog bone" shaped samples for mechanical testing. The gage length was 19mm, the width 6.4 mm, and the thickness the same as that of the rolled sample, 0.50 mm. These were then tested in tension to failure at a strain rate of $8.8 \times 10^{-4} \text{ s}^{-1}$ and subsequently mounted and polished for optical microscopy.

In addition to samples containing 15 v/o second phase, a 6 g sample with 24 v/o Al₃Zr_{0.25}Ti_{0.75} was prepared by arc-melting. It also was annealed at 500 °C for one hour and hot-pressed at 500 °C to a final reduction of 60%. A regimen of cold-rolling with intermittent annealing at 400 °C, similar to that followed for the 15 v/o samples, produced a sample 0.50 mm thick (a total reduction in thickness of 95%).

3. Results

The intermetallic particles in the as-cast structure are plate-like: the largest ones are over 200 μm long and 75 μm wide but only 6 μm thick (see Figure 1); the average aspect ratio (length/thickness *in the long transverse plane*) is 27; length is measured parallel to the long axes of the figures. They are tetragonal, of the D0₂₃ structure, as confirmed by x-ray diffractometry.

Figure 2 represents a long transverse section of the hot pressed sample (sample I). Some of the particles are greater than 100 μm long but no greater than 6 μm thick; the *average* aspect ratio is 9.5. Several particles are curved, indicating plasticity of the intermetallic particles at the hot-pressing temperature (500 °C). This is should be contrasted to the work of Yamaguchi, *et al.* on polycrystalline Al₃Ti which indicates the onset of plasticity in this intermetallic is at 620 °C (3).

Longitudinal and long transverse sections of the sample cold-rolled to 95% reduction (sample II) are shown in Figure 3. The particles have been reduced considerably in size: in the rolling plane, the platelets have widths of up to 80 μm , although most have widths no greater than 15 μm . In transverse section, it is clear that rolling has dramatically decreased the aspect ratios of the particles; the average value is 4.9. Interestingly though, there is no evidence of particle/matrix separation due to the cold rolling.

Transverse sections of samples III and IV demonstrate that additional cold-rolling serves to further break-up the particles. In sample III (Figure 4) the average particle aspect ratio is 2.7. In sample IV (Figure 5), it is 2.6. In sample IV, the ability of the matrix material to flow around the particles is indicated. The interface still appears to be continuous. After no stage of deformation was interface decohesion observed. The wavy dark lines in Figure 5 arise from the "mille feuille" structure of the rolled and folded sample.

All of the micrographs show that the particle/matrix interface has the ability to "heal" after severe deformation, even though the particles are fractured. In the as-cast structure, the particles are long and thin. Cold-rolling effectively breaks up the particles into smaller pieces. Between these new pieces, the aluminum matrix apparently flows and fills in the space created when the particles move apart from each other and bonds to the particles. The thickness of the particles, though, does not change during the deformation sequence: in the as-cast composite, the median particle thickness is $5 \pm 2 \mu\text{m}$; in the sample rolled to 99.983% reduction, it is $5 \pm 3 \mu\text{m}$. Thus, the particle/matrix interface in the longitudinal plane is presumably the same as that in the as-cast composite.

Figures 6a and 6b show longitudinal sections of one of the samples tested in tension to failure. Some interfacial debonding is seen in the vicinity of the fracture surface (Figure 6a). At the fracture surface (Figure 6b), fracture has occurred at a particle/matrix interface, but at other particles a thin layer of aluminum matrix remains at the interface.

It is suggested that the ductility of the Al/Al₃Zr_{0.25}Ti_{0.75} metal-matrix composite is due to the inherent properties of the particle/matrix interface. After severe deformation of the composite material, the interface appears to be continuous; no particle fallout was observed. However, further testing will be necessary to determine the microscopic nature of the particle/matrix interface. Specifically, high-resolution electron microscopy of the interface would indicate the nature of the interfacial bonding. Additionally, while increased deformation of the sample has consistently reduced the average particle aspect ratio, plasticity of the intermetallic particles at room temperature, which would contribute to the overall ductility of the composite, can not be ruled out.

4. Summary

The Al/Al₃Zr_{0.25}Ti_{0.75} and Al/Al₃Zr_{0.25}Ti_{0.75} metal-matrix composites have shown unusual ductility. A sample containing 15 v/o of the intermetallic Al₃Zr_{0.25}Ti_{0.75} has been successfully hot-pressed and cold-rolled to a total reduction in thickness of some 99.98% without intermediate anneals. A composite with 24 v/o of

$\text{Al}_3\text{Zr}_{0.75}\text{Ti}_{0.25}$ has been rolled to a 95% reduction. The proposed reasons for the ductility are the plasticity of the intermetallic particles at 500 °C, the lack of brittleness of the particle/matrix interface, and its ability to heal. This composite is prepared by solidification of a molten mixture of its elemental constituents. Thus, it can be prepared by conventional casting and thermomechanical processing.

By suitable alloying to strengthen its matrix, the $\text{Al}/\text{Al}_3\text{Zr}_x\text{Ti}_{1-x}$ system may be the basis for development of a useful metal-matrix composite by conventional ingot metallurgy processing.

Acknowledgement

This research was supported by the Air Force Office of Scientific Research grant number AFOSR 89-0043 under the direction of Dr. Alan Rosenstein.

1. G. Brauer, *Z. Anorg. allg. Chem.* **242**, 1 (1939).
2. S. Tsunekawa and M. E. Fine, *Scripta Met.* **16**, 391 (1982).
3. M. Yamaguchi, Y. Umakoshi, and T. Yamane, *Phil. Mag. A* **55**, 301 (1987).



Fig. 1. As-cast microstructure.



Fig. 2. Sample I: hot-pressed to 59 % total reduction in thickness. Long transverse section. Arrows indicate apparent ductility of intermetallic particle.



Fig. 3. Sample II: cold-rolled to 95% total reduction in thickness. a) Longitudinal section. b) Long transverse section.



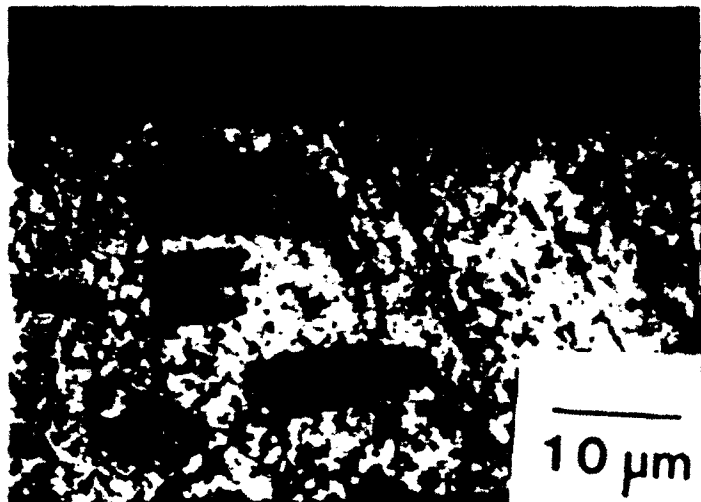


Fig. 4. Sample III: cold-rolled to 99.74% total reduction in thickness. Long transverse section.



Fig. 5. Sample IV: cold-rolled to 99.983% total reduction in thickness. Long transverse section.



a)



b)

Fig. 6. Cold-rolled to 95% total reduction in thickness. Tested in tension to failure. Longitudinal section. a) Region adjacent to fracture surface. Arrows indicate voids at particle/matrix interface. b) Fracture surface. Arrows indicate thin layer of aluminum at particle/matrix interface.